



ELSEVIER

Physica D 2801 (2001) 1–25

PHYSICA D

www.elsevier.com/locate/physd

A Boolean delay equations model of ENSO variability

Amira Saunders*, Michael Ghil

*Department of Atmospheric Sciences, Institute of Geophysics and Planetary Physics, University of California Los Angeles,
Los Angeles, CA 90095-1565, USA*

Received 5 May 2000; received in revised form 10 June 2001; accepted 30 July 2001

Communicated by U. Frisch

Abstract

Boolean delay equations (BDEs) provide a mathematical framework to formulate and analyze conceptual models of complex multi-component systems. This framework is used here to construct a simple conceptual model for the El-Niño/Southern Oscillation (ENSO) phenomenon. ENSO involves the coupling of atmospheric and oceanic processes that are far from being completely understood. Our BDE model uses *Boolean* variables to represent key atmospheric and oceanic quantities and equations that involve *logical* operators to describe their evolution. Two distinct time-delay parameters, one for the local atmosphere–ocean coupling effects and the other for oceanic wave propagation, are introduced.

Over a range of physically relevant delay values, this truly minimal model captures two essential features of ENSO’s interannual variability — its regularity and its tendency to phase-lock to the annual cycle. Oscillations with average cycle length that is an integer multiple of the seasonal cycle are prevalent and range from 2 to 7 years. Transition zones — where the average period lengths are noninteger rational multiples of the forcing period — exhibit Devil’s staircases, a signature of the quasi-periodic (QP) route to chaos. Our BDE model thus validates results from previous studies of the interaction of the seasonal cycle with ENSO’s “delayed oscillator”. It gives therewith support to the view that the observed irregularity results predominantly from low-order chaotic processes rather than from stochastic weather noise.

Moreover, in the transition zone between the two integer periodicities of 2 and 3 years, a heretofore unsuspected, self-similar “fractal sunburst” pattern emerges in phase-parameter space. This pattern provides a distinct and more complex scenario than the QP route to chaos found in earlier, more detailed ENSO models. Period selection in this 2–3-year transitional region seems to play a key role in ENSO’s irregularity, as well as in the appearance of the observed quasi-biennial mode of variability. © 2001 Published by Elsevier Science B.V.

Keywords: Cellular automata; Delay equations; Devil’s staircase; El Niño; Frequency locking; Hierarchical modeling

1. Introduction

The El-Niño/Southern Oscillation (ENSO) phenomenon is the most prominent signal of seasonal-to-interannual climate variability and has been the focus of intense research in the last two decades. The phe-

nomenon was known for centuries to fishermen along the west coast of South America, who witnessed a seemingly sporadic and abrupt warming of the cold, nutrient-rich waters that caused havoc to their fish harvests [1,2]. Its common occurrence shortly after Christmas inspired them to name it El Niño, after the “Christ child”. Starting in the 1970s, El Niño’s climatic effects were found to be far broader than just its off-shore manifestations. Measurements have shown

* Corresponding author. Fax: +1-310-206-5219.
E-mail address: amira@atmos.ucla.edu (A. Saunders).

45 it to have spatial coherence spanning vast distances
46 across the entire tropical Pacific Ocean [3,4]. Beyond
47 that, harder to document “teleconnections” [5] may
48 cause increased storm activity and precipitation in
49 some areas of the globe and drought in others [6],
50 with effects reaching as far as Alaska and the Indian
51 Ocean. These effects have led to a global awareness
52 of ENSO’s significance, and an impetus to attempt
53 and improve predictions [7].

54 Bjerknes [8] laid the foundation of modern ENSO
55 research by proposing that it arises as a natural
56 intrinsic oscillation of the air–sea system in the
57 tropics. His ideas established the need for *coupled*
58 atmosphere–ocean models. Thereafter, progress in ex-
59 ploring ENSO’s variability was made by employing
60 an extensive hierarchy of dynamical models [9,10].
61 Detailed ENSO simulations are mainly carried out by
62 coupled general circulation models (GCMs) of both
63 the atmosphere and the ocean [11,12], while extremely
64 idealized conceptual models, sometimes dubbed “toy
65 models” [13–15], proved instrumental in understand-
66 ing the basic underlying physical mechanisms that
67 drive the oscillation. These two ends of the modeling
68 hierarchy are bridged by so-called intermediate mod-
69 els that include some ad hoc assumptions [16–18].

70 ENSO variations are a part of the climate system’s
71 seasonal-to-interannual variability and are dominated
72 by complex feedbacks between subsystems active on
73 different time scales. ENSO exhibits some degree of
74 periodicity and is phase-locked to the annual cycle to a
75 certain extent. It also possesses, however, an enigmatic
76 irregularity that renders it a modeling and forecasting
77 challenge [7,19,20]. Its complexity has inspired the in-
78 troduction of new types of models, such as neural net-
79 works [21,22], and of new techniques for data analysis,
80 such as wavelets [23] and singular spectrum analysis
81 (SSA [24,25]) into climate dynamics. ENSO research
82 has thus become a frontier of climate studies, where
83 results obtained by classical and by less traditional ap-
84 proaches can be usefully compared to each other.

85 Boolean delay equations (BDEs) are a novel mod-
86 eling language especially tailored for the formal ex-
87 pression of conceptual models of systems that exhibit
88 threshold behavior, multiple feedbacks and distinct
89 time delays. Originally inspired by theoretical biol-

ogy [26,27], Ghil and co-workers [28,29] recognized 90
the potential of BDEs for modeling the multiple feed- 91
backs between the components of the climate system. 92
They intended BDEs as a heuristic first step on the 93
way to understanding problems too complex to model 94
using systems of partial differential equations (PDEs) 95
at the present time. One hopes, of course, to be able to 96
eventually write down and solve the exact equations 97
that govern the most intricate phenomena. Still, in cli- 98
mate dynamics and elsewhere in the natural sciences, 99
much of the preliminary discourse is often conceptual. 100
BDEs offer a formal mathematical language that may 101
help bridge the gap between qualitative and quantita- 102
tive reasoning. This study was motivated by the dual 103
aspiration of gaining further insight into the climatic 104
phenomena of interest, as well as into the modeling 105
tool’s mathematical properties. 106

107 The ENSO phenomenon has been extensively stud-
108 ied using a full hierarchy of climate models that
109 range from simple toy models, governed by one or a
110 few ordinary or delay differential equations (DDEs),
111 to fully coupled GCMs [9,10,20]. In such a frame-
112 work, simple conceptual models are typically used
113 to present hypotheses and investigate isolated mech-
114 anisms, while more detailed models try to simulate
115 the phenomena more realistically and test for the ef-
116 fect of the suggested mechanisms. Our BDE model
117 may be the simplest representation so far of the
118 “delayed-oscillator” concept in the tropical Pacific’s
119 coupled ocean–atmosphere system and of its inter-
120 action with the seasonal cycle. In the true spirit of
121 advancing our knowledge by moving across a hierar-
122 chy of models, some of our results validate those dis-
123 covered using significantly more complex, smoothly
124 differentiable models. At the same time, new results
125 obtained with our BDE model capture phenomena
126 not yet detected using more conventional tools. These
127 results suggest a possible mechanism for ENSO’s
128 period selection that may be investigated using more
129 complex models once its “blueprint” was seen in a
130 simple conceptual model.

131 The outline of this paper is as follows. In Section 2,
132 we present a short introduction to BDEs: their moti-
133 vation, general form, and some theoretical results that
134 will be useful for understanding our ENSO model’s

135 behavior. We also mention some previous applications
136 to climate problems on different time scales.

137 In Section 3, we formulate a simple BDE model for
138 ENSO: we discuss first the feedback mechanisms that
139 are modeled, while at the same time reviewing a few
140 analog toy models. We then present our model’s vari-
141 ables and the equations that determine their evolution,
142 given two distinct delays: one associated with cross-
143 basin travel time of waves in the equatorial duct,
144 the other with local ocean–atmosphere processes.
145 Appendix A discusses the numerical aspects of the
146 model’s formulation: we outline the algorithm used
147 to obtain time-evolving solutions for different delay-
148 parameter values and its numerical implementation.

149 In Section 4, we present and classify the solu-
150 tions according to their complexity by using a novel
151 pattern recognition scheme. A “Devil’s staircase”
152 emerges when plotting the period against the wave
153 delay, while keeping the local-delay parameter
154 fixed. Separate staircases can then be represented as
155 “Devil’s bleachers” or a “Devil’s terrace” [30] in the
156 three-dimensional space of the two parameters and
157 the “period”. The universal quasi-periodic (QP) route
158 to chaos is thus present in our BDE model and we
159 compare its results to the earlier ones obtained by us-
160 ing simple and intermediate models that are governed
161 by differential, DDEs or PDEs.

162 Between the two broad integer steps at 2 and 3 years,
163 the BDE model diverges from the classical scenario
164 as a telescoping, self-similar “fractal sunburst” pattern
165 appears embedded in the Devil’s staircase. This newly
166 found behavior is more complex than previously ob-
167 served. It points to a new, deterministic scenario for
168 the variations in ENSO’s period selection in this pa-
169 rameter region. A deeper understanding of this behav-
170 ior seems pivotal to explaining the coexistence of a
171 broad quasi-biennial peak in ENSO variability [24,25]
172 with the irregular occurrence of extreme events.

In Section 5, we discuss our results more broadly in
the context of the intriguing complementarity between
the regularity and irregularity of the ENSO phenom-
ena. We compare our results with other modeling and
observational studies that point to low-dimensional
chaos induced by resonances between the frequencies
of ENSO’s internal oscillator and the annual cycle.
This is followed by further remarks concerning the
new types of BDE behavior found in the present study.
We conclude by discussing future extensions of BDE
theory and its applications to ENSO and to other cli-
mate problems.

2. Boolean delay equations

2.1. Motivation

BDEs may be classified as *semi-discrete dynamical*
systems, where the dependent variables are discrete —
typically Boolean, i.e., taking the values 0 (“on”) or 1
 (“off”) only — while time is allowed to be continuous.
As such they occupy the previously “missing entry”
in Table 1 where dynamical systems are classified ac-
cording to whether their time (t) and state variables
(\vec{x}) are continuous or discrete.

Systems in which both the variables and time are
continuous are called *flows* [32,33] (upper left entry).
Vector fields, ordinary differential equations (ODEs)
and PDEs, functional differential equations (FDEs)
and DDEs and stochastic differential equations (SDEs)
belong to this category.

Systems with continuous variables and discrete time
(upper right), are known as *maps* [34,35] and include
Poincaré maps, as well as ordinary and partial differ-
ence equations (O Δ Es, P Δ Es). *Automata* (lower right
entry) have discrete time and variables: cellular au-
tomata (CAs) and all Turing machines (including com-

Table 1
Classification of dynamical systems

	t continuous	t discrete
\vec{x} continuous	Flows: vector fields, ODEs, PDEs, FDEs, DDEs, SDEs	Maps: Poincaré maps (O Δ Es, P Δ Es)
\vec{x} discrete	BDEs: kinetic logic conservative logic	Automata: Turing machines, CAs

207 puters) are part of this group [36,37]. BDEs and their
 208 predecessors, kinetic and conservative logic, com-
 209 plete the table and occupy the remaining bottom left
 210 entry.

211 The primary motivation that led Ghil and co-workers
 212 [28,29] to formulate BDEs was their desire to analyze
 213 in a more precise way the implications of descrip-
 214 tive conceptual models prevalent in the interpretation
 215 of paleoclimate records [38–40]. Further inspiration
 216 came from advances in theoretical biology, following
 217 upon Jacob and Monod’s discovery [26] of on–off
 218 interactions between genes, which had prompted the
 219 formulation of “kinetic logic” [27,41] and Boolean
 220 regulatory networks [42]. As the study of complex
 221 systems garners increasing attention and is applied
 222 to diverse areas—from economics to the evolution
 223 of civilizations, passing through physics—related
 224 Boolean and other discrete models are being explored
 225 more and more [36,43,44].

226 *2.2. General form*

227 Given a system with n continuous real-valued state
 228 variables $\vec{v} = (v_1, v_2, \dots, v_n) \in \mathcal{R}^n$ for which natural
 229 thresholds $q_i \in \mathcal{R}$ exist, one can associate with each
 230 variable $v_i \in \mathcal{R}$ a Boolean-valued variable, $x_i \in \mathcal{B} =$
 231 $\{0, 1\}$, i.e., a variable that is either “on” or “off,” by
 232 letting

$$233 \quad x_i = \begin{cases} 0, & v_i \leq q_i, \quad i = 1, \dots, n, \\ 1, & v_i > q_i, \quad i = 1, \dots, n. \end{cases} \quad (1)$$

234 We are interested in the evolution of the Boolean vec-
 235 tor $\vec{x} = (x_1, x_2, \dots, x_n) \in \mathcal{B}^n$ due to time-delayed in-
 236 teractions between the Boolean variables $x_i \in \mathcal{B}$. This
 237 evolution can be described by a set equations that take
 238 the form

$$239 \quad \begin{aligned} x_1 &= f_1(x_1(t - \theta_{1,1}), x_2(t - \theta_{1,2}), \dots, x_n(t - \theta_{1,n})), \\ x_2 &= f_2(x_1(t - \theta_{2,1}), x_2(t - \theta_{2,2}), \dots, x_n(t - \theta_{2,n})), \\ &\vdots \\ &\vdots \\ 240 \quad x_n &= f_n(x_1(t - \theta_{n,1}), x_2(t - \theta_{n,2}), \dots, x_n(t - \theta_{n,n})). \end{aligned} \quad (2)$$

241

242 The functions $f_i : \mathcal{B}^n \rightarrow \mathcal{B}$, $1 \leq i \leq n$, are defined
 243 via Boolean equations that involve logical operators
 244 and delays. Each delay value $\theta_{i,j} \in \mathcal{R}$, where $1 \leq i$,
 245 $j \leq n$, is the length of time it takes for a change in
 246 variable x_j to affect the variable x_i .

247 *2.3. Some theoretical and numerical results*

248 We summarize here a few basic theoretical results
 249 from BDE theory that help understand our ENSO
 250 model results. Their original form appears in Ghil and
 251 Mullhaupt [29]. They are followed by some simple
 252 numerical considerations.

253 *2.3.1. Existence and uniqueness of solutions*

254 Given a BDE system (2) as above and initial data
 255 that are piecewise-constant over an interval equal in
 256 length to the longest delay, one can prove by construc-
 257 tion the existence of a unique solution [28]. In essence,
 258 the time evolution can be traced arbitrarily far into the
 259 future, by sliding the finite-length “memory window”
 260 of the system along the time axis. The existence proof
 261 hinges on a result that follows from the “pigeon-hole”
 262 lemma stated below. One obtains therefrom that only
 263 a finite number of “jumps” (between 0 and 1) can oc-
 264 cur in any finite-time interval.

265 *2.3.2. “Pigeon-hole” lemma*

266 All BDE systems with *rational* delays can be re-
 267 duced in effect to finite CAs; see Table 1. Commen-
 268 surability of the delays creates a partition of the time
 269 axis into segments over which state variables remain
 270 constant and whose length is an integer multiple of the
 271 delays’ least common denominator. As there is only a
 272 finite number of possible assignments of two values to
 273 these segments, repetition must occur. Hence the only
 274 asymptotic behavior possible is eventual constancy or
 275 periodicity in time.

276 *2.3.3. Classification*

277 Based on Section 2.3.2, Ghil and Mullhaupt [29]
 278 classified BDE systems into two types. All systems
 279 with solutions that are immediately periodic for all
 280 rational delays are *conservative*. Any system that for
 281 some rational delays exhibits transient behavior be-

fore settling into eventual periodicity is *dissipative*.
 The obvious analogy with differentiable dynamical systems is with conservative (e.g., Hamiltonian) systems [45] versus forced-dissipative systems (e.g., the well-known Lorenz [46] system).

2.3.4. Asymptotic behavior

The following types of asymptotic behavior were observed in BDE systems prior to this study: (a) fixed point—the solution reaches one of a finite number of possible states and remains there; (b) limit cycle—the solution becomes periodic after a finite-time elapses; (c) growing complexity—certain classes of BDEs with incommensurable delays were shown to have solutions with growing complexity, as measured by the number of jumps per unit time. Examples were shown where the growth in complexity is essentially log-periodic [28,29].

2.3.5. Approximation theorem

All solutions to systems of BDEs can be approximated (with respect to an \mathcal{L}_2 -norm) for a given finite time by the periodic solutions of a nearby system having rational delays only.

2.3.6. Numerical considerations

The details of the forward-stepping algorithm for obtaining solutions are provided in Appendix A.1. In actuality, the solutions may be sensitive to round-off errors, as a reordering of jump points may alter a solution's qualitative behavior. A numerical implementation of the algorithm especially designed to circumvent this obstacle is outlined in Appendix A.2.

A related numerical difficulty arises as irrational delays cannot be represented on finite-precision digital computers. Ghil and Mullhaupt [29] developed a method that was particularly suitable for certain classes of BDE systems. In their method, computations were carried on a delay lattice constructed of all possible jump points, and an analytical criterion was used to determine which lattice points correspond to an actual jump. Those lattice points were then projected onto the time axis to yield the correct order of jumps.

For all BDE systems that are not amenable to the delay-lattice method of [29], the above approximation theorem allows one to investigate their behavior when the delays are not rationally related. The theorem ensures that, even aperiodic solutions can be captured to within arbitrary precision and for an arbitrary (but finite) length of time. This is done by using easily computable periodic solutions of systems that have rational delays, close to the irrational ones that are being approximated. As the rational approximation of the irrational delays improves, the period of the computed solution increases and so does the time interval for which the approximation is valid.

2.4. Applications to climate problems

The climate system presents a complex challenge to modelers as it consists of a number of subsystems with multiple feedbacks that act on different time scales [47–49]. The exact physical nature of many of these processes and the relevant values of the parameters involved are in many cases unknown; it is often difficult, therefore, to construct appropriate models based on differential equations [41,50]. Arguably, it is most important to determine which components and feedbacks are crucial for the understanding of a specific problem and to obtain a rough estimate of the thresholds and time delays associated with them. This information suffices to construct a BDE model of the problem. A theoretical investigation of this model then yields qualitative and semi-quantitative results on the possible outcomes of the above assumptions and approximate determinations [51–53].

BDEs were first applied to the paleoclimate problem of *Quaternary glaciation cycles* and their relationship to changes in the deep ocean's overturning circulation on *multi-millennial* time scales [51,52]. Next, Darby and Mysak [53] constructed a model for the evolution of the North Atlantic ocean's Great Salinity Anomaly as part of an *interdecadal* Arctic climate cycle. In the following section, we present a BDE model for ENSO—thus applying BDEs to *interannual* climate variability.

367 **3. A BDE model for ENSO**368 *3.1. Conceptual ingredients*

369 The following conceptual elements are incorporated
370 into the logical equations of our BDE model for ENSO
371 variability.

372 *3.1.1. The Bjerknes hypothesis*

373 Bjerknes [8] suggested a *positive feedback* as a
374 mechanism for the growth of an internal instability
375 in the tropical *air–sea* system. The “chain reaction”
376 starts with an initial warming of sea-surface temper-
377 atures (SSTs) in the “cold tongue” that occupies the
378 eastern part of the equatorial Pacific [1]. This warming
379 causes a weakening of the thermally driven, East–West
380 oriented Walker-cell circulation. As the trade winds
381 blowing from the east subside, they give way to west-
382 erly (i.e., eastward blowing) wind anomalies; in me-
383 teorological parlance, an *anomaly* is simply the dif-
384 ference between the instantaneous value or short-term
385 mean of a given field and its long-term or *climato-*
386 *logical* mean. The ensuing local changes in the ocean
387 circulation encourage further SST increase. Thus the
388 “loop” is closed and further amplification of the insta-
389 bility is “triggered”.

390 *3.1.2. Delayed oceanic wave adjustments*

391 Compensating for Bjerknes’s positive feedback is a
392 *negative feedback* in the system that allows a return to
393 colder conditions in the basin’s eastern part. During
394 the peak of the cold-tongue warming, called the warm
395 or El Niño phase of ENSO, westerly wind anomalies
396 prevail in the central part of the basin. As part of
397 the ocean’s adjustment to this atmospheric forcing, a
398 Kelvin wave is set up and carries a warming signal
399 eastward. This signal deepens the thermocline—
400 i.e., the interface that separates the near-surface
401 well-mixed, warmer waters from the colder, more
402 stratified waters underneath—in the eastern portion
403 of the basin and contributes to the positive feedback
404 described above. Concurrently, slower Rossby waves
405 propagate westward, and are reflected at the basin’s
406 western boundary. This reflection gives rise to an
407 eastward-propagating Kelvin wave that has a cooling,

thermocline-shoaling effect. Over time, the arrival of 408
this signal erodes the warm event, ultimately causing 409
a switch to a cold, La Niña phase. 410

The interplay of local air–sea interaction in the east- 411
ern tropical Pacific with wave propagation across the 412
basin was originally introduced by Schopf and Suarez 413
[13] and Battisti and Hirst [14] into their “toy models”. 414
The latter were devised to help explain the results 415
of their respective more realistic and detailed ENSO 416
models. These toy models were formulated as a scalar 417
differential-delay equation [54] for a variable T that 418
denotes sea-surface temperature anomalies (SSTAs) in 419
the eastern part of the tropical Pacific, and were of the 420
form 421

$$\frac{dT}{dt} = \alpha T - \delta(t - \tau) - \gamma T^3. \quad (3) \quad 422$$

The term αT on the right-hand side stands for growth 423
or decay of the anomaly due to local processes that 424
carry out the Bjerknes positive feedback. The term 425
 $-\delta(t - \tau)$ represents the weighted wave-delayed ef- 426
fects and the term $-\gamma T^3$ represents limiting nonlinear- 427
ities. Similar differential-delay models had been for- 428
mulated for paleoclimate problems by Bhattacharya 429
et al. [55]. 430

Schopf and Suarez [13] examined the region in the 431
parameter space where $\alpha > \delta$ and thus local effects are 432
stronger than wave effects. They found that—while 433
the wave delay τ is small—there is but one stable 434
solution, $T = 0$, and it corresponds to the system’s 435
“climate”. As the wave delay is increased, this solu- 436
tion loses its stability and two other stable steady-state 437
solutions emerge; they correspond, in principle, to El 438
Niño and La Niña. 439

Battisti and Hirst [14], on the other hand, concen- 440
trated on the region $\alpha < \delta$ and found that a Hopf 441
bifurcation occurs when the initially stable solution 442
 $T = 0$ loses its stability to periodic solutions, as 443
the wave delay is increased. Later, Jin and Neelin 444
[18,56] used a simplified version of the intermediate 445
coupled model of Cane and Zebiak [16] to show that 446
ENSO does indeed arise in that model as the first Hopf 447
bifurcation from the climate steady state. Thus the 448
“multiple-equilibria” hypothesis was eliminated and 449
parameter regimes where wave effects dominate local 450

451 processes were established as the relevant ones for the
452 above differential-delay models.

453 Since this wave delay mechanism was first formu-
454 lated, it became clear that it describes but one limit
455 of interest in the coupled ocean–atmosphere system’s
456 parameter space, whereas a more complete descrip-
457 tion should include surface-layer oceanic adjustments
458 as well [18,56–58]. Jin [59] has suggested a wider
459 interpretation of the “delayed action” to include other
460 oceanic processes that may be contributing to the
461 system’s memory, such as replenishment of heat con-
462 tent in the warm pool of the western tropical Pacific.
463 We rely, in that vein, on the basic delayed-oscillator
464 concept, essential for understanding ENSO cyclicity,
465 and bear in mind that the wave-packet propagation
466 [13,14] described above is but a crude yet useful
467 metaphor for a more general delay mechanism.

468 3.1.3. Seasonal forcing

469 A growing body of work [30,60–64] points to res-
470 onances between the Pacific basin’s air–sea oscillator
471 and the annual cycle as a possible cause for the ten-
472 dency of warm events to peak in boreal winter, as well
473 as for ENSO’s intriguing mix of temporal regularities
474 and irregularities. The mechanisms by which this in-
475 teraction takes place are numerous and intricate and
476 their relative importance is not yet fully understood
477 [17,64]. We assume, therefore, in the present simple
478 BDE model that the climatological annual cycle pro-
479 vides for a seasonally varying potential of event am-
480 plification.

481 3.2. Model variables

482 3.2.1. Oceanic variables

483 The state of the ocean is depicted by SSTAs aver-
484 aged over the Niño-3 region in the eastern equatorial
485 Pacific (5°S–5°N, 150–90°W) [1]. The mean SSTA
486 in this region is often used to characterize the phase
487 of the ENSO oscillation [1,31,67]. The formulation of
488 a minimal BDE system rich enough to describe the
489 above conceptual interactions requires us to differen-
490 tiate, at least, between mild and extreme conditions.
491 To that end, a combination of two Boolean variables,
492 T_1 and T_2 , is used to create four possible states de-

Table 2
Truth table for SSTAs

T_1	T_2	SSTA conditions
0	0	Extremely cold SSTA — La Niña
0	1	Mild cold SSTA
1	0	Mild warm SSTA
1	1	Extremely warm SSTA — El Niño

493 scribing Niño-3 SSTAs: T_1 equals 0 or 1 when cold or
494 warm anomalies are present, and thus corresponds to
495 the sign of the anomalies; T_2 equals T_1 if the anomaly
496 on hand is extreme, or takes on the opposite value if
497 the event is mild, and thus indicates the amplitude of
498 the anomalies. The resulting “extended truth table” for
499 Niño-3 SSTA is given in Table 2.

500 3.2.2. Atmospheric variables

501 The relevant anomalous atmospheric conditions in
502 the Equatorial Pacific basin are represented by binning
503 the near-surface wind-stress anomalies in the central
504 equatorial Pacific (5°S–5°N, 175–140°W) also into
505 four levels, described by the variables U_1 and U_2 : U_1
506 corresponds to the direction of the winds and is equal
507 to 1 when the wind anomalies are westerly and 0 when
508 they are easterly; U_2 is equal to U_1 when the wind
509 conditions are extreme and $U_1 \neq U_2$ when they are
510 mild. Thus zonal wind-stress anomalies in the central
511 Pacific are classified in Table 3 as being in one of the
512 four discrete states.

513 3.2.3. Seasonal-cycle variable

514 The seasonal cycle’s external forcing is represented
515 by a two-level Boolean variable S . This variable as-
516 sumes the value 0 or 1 according to whether it is the
517 amplification of a cold or a warm event that is favored.
518 Unlike the oceanic and atmospheric variables that are
519 *internal*, S is able to affect the evolution of the sys-

Table 3
Truth table for surface winds

U_1	U_2	Wind conditions
0	0	Extreme easterly anomalies
0	1	Mild easterly anomalies
1	0	Mild westerly anomalies
1	1	Extreme westerly anomalies

tem, but is not affected by it, and thus is considered external. This represents an innovation in the study of BDEs, where only autonomous systems, without time-varying forcing, had been considered before.

3.3. Model equations

The atmospheric variables U_1 and U_2 encapsulate the atmospheric response to the ocean's SSTAs. This response is known to be quite rapid when compared to the ocean's evolution. Therefore, as appropriate for a first approximation, U_1 and U_2 are modeled as "slaved" to the ocean:

$$U_1(t) = T_1(t - \beta), \tag{4}$$

$$U_2(t) = T_2(t - \beta). \tag{5}$$

This type of slaving was also used in more detailed and realistic ENSO models [9,30]. The changes in wind conditions are assumed to lag the SSTA variables by a short delay β , of the order of days to weeks. For simplicity, all other time lags associated with local coupled adjustment processes are also assumed to equal β . We model next the evolution of the sign T_1 of SSTAs by letting one of the two possible sets of delayed interactions play a role:

1. Extremely anomalous wind-stress conditions are assumed to be necessary to generate a significant Rossby-wave signal $R(t)$; this signal takes on the value 1 when wind conditions are extreme at the time and 0 otherwise. By definition, strong wind anomalies (either easterly or westerly) prevail when $U_1 = U_2$ and thus $R(t) = U_1(t) \Delta U_2(t)$; here Δ is the binary Boolean operator that takes on the value 1 if and only if both operands have the same value. A wave signal $R(t) = 1$ that is elicited at time t is assumed to re-enter the model system after a delay τ , associated with the wave's travel time across the basin. Upon arrival of the signal in the eastern equatorial Pacific at time $t + \tau$, the wave signal affects the thermocline-depth anomaly there and thus reverses the sign of SSTAs represented by T_1 .

The length of the delay τ is in the order of months, if one interprets it as the travel time of the

gravest Rossby-wave mode. Idealized models [1] yield a value for this travel time that equals approximately 6 months. We may however adopt Jin's [59] broader view of the delayed-oscillator mechanism and let τ represent the time that elapses, while combined processes of oceanic adjustment occur. In that case, τ should be allowed a broader range and can also be assumed to be subject to slow changes in time.

2. In the second set of circumstances, when $R(t) = 0$, and thus no significant wave signal is present, we assume that $T_1(t + \tau)$ responds directly to local atmospheric conditions, after a delay β , according to Bjerknes's hypothesis.

The two mechanisms (1) and (2) are combined to yield

$$T_1(t) = \{(R \wedge \neg U_1)(t - \tau) \vee \{\neg R(t - \tau) \wedge U_2(t - \beta)\}, \tag{6}$$

where the symbols \vee and \wedge represent the binary logical operator OR and AND, respectively.

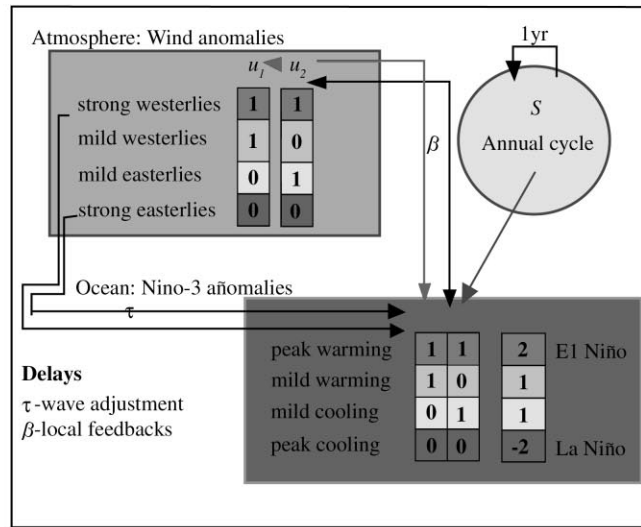
The seasonal-cycle forcing S is allowed to evolve by mandating simply that the climatic information supplied in the initial data is carried forward by S from year to year. The time unit is taken to equal one year, thus yielding

$$S(t) = S(t - 1). \tag{7}$$

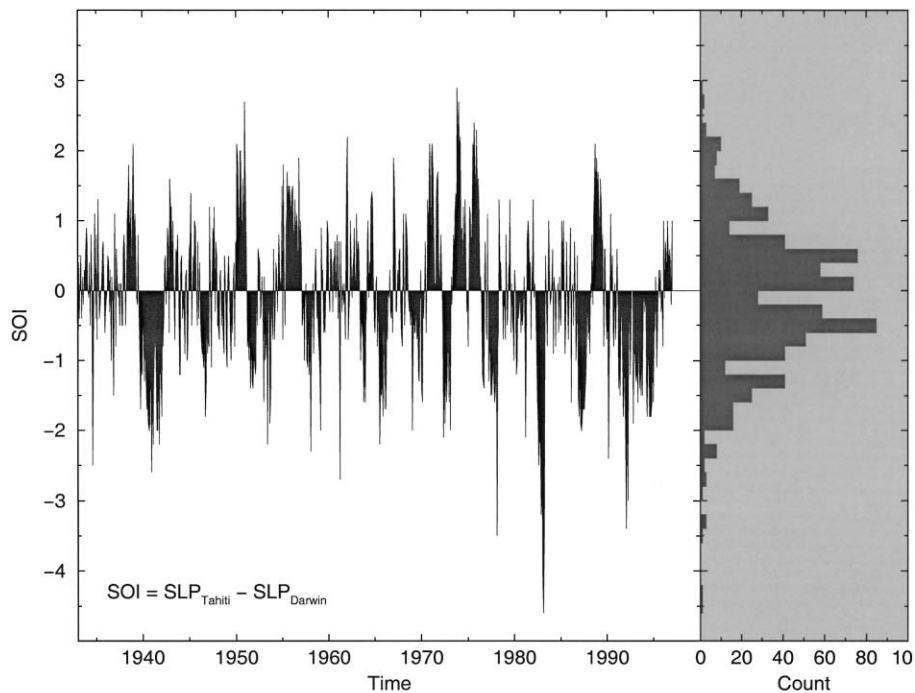
The forcing represented by S affects the SSTA amplitude T_2 through an enhancement of events when favorable seasonal conditions prevail:

$$T_2(t) = \{[S \Delta T_1](t - \beta) \vee \{[\neg(S \Delta T_1) \wedge T_2](t - \beta)\}. \tag{8}$$

Fig. 1a presents a schematic diagram of system variables and their interactions. It also depicts a mapping of the SSTA states represented by the two-variable Boolean vector (T_1, T_2) into a single, four-level scalar variable. We named this scalar "ENSO" to signify extreme and mild La Niña, mild and extreme El Niño conditions, in this order, with values $\{-2, -1, 1, 2\}$ respectively, cf. [65,66]; see also Fig. 1b.



(a)



(b)

Fig. 1. Model formulation. (a) A schematic diagram of our BDEs model for ENSO. An arrow that points from variable A to variable B indicates that a jump in A may cause a jump in B after the time delay indicated on the shaft of the arrow. (b) Why four levels? The Southern Oscillation index (SOI) is defined as the difference between the time series of monthly mean sea level pressure at Tahiti and Darwin. These two time series are each centered and normalized by its standard deviation, respectively. The SOI is widely used to represent the conditions in the Equatorial Pacific. It is strongly anti-correlated with the other index that is widely used to characterize the tropical Pacific's overall state and is called "Niño-3" (see text and Fig. 1a for details): when SSTAs in the Niño-3 region of the eastern equatorial Pacific are positive, the SOI is negative, and vice-versa. The SOI time series in this panel, together with the accompanying histogram (courtesy of P. Yiou), support the existence of four natural discrete levels, as used in panel (a). The four discrete the Niño-3 region of the eastern equatorial Pacific are positive, the SOI is negative, and vice-versa. The SOI time series in this panel, together with the accompanying histogram (courtesy of P. Yiou), support the existence of four natural discrete levels, as used in panel (a). The four discrete states are separated by gaps in the histogram that are located near zero and ± 1 standard deviation. The position of these gaps motivates the association of the four states with the $\{-2, -1, 1, 2\}$ levels of strong and mild La Niña and mild and strong El Niño used in the BDE model.

602 3.4. Initial data and parameter values

603 We prescribe initial data for our BDE model over
604 a 2-year interval that describes the early part of a
605 “canonical” ENSO scenario, according to the com-
606 posite event that was constructed by Rasmusson and
607 Carpenter [67] based on six warm events between the
608 years 1953 and 1973.

609 We have also used as initial data certain observa-
610 tional data segments, prior to selected warm events,
611 that were discretized by setting threshold values de-
612 termined by the standard deviations. We assume that
613 late boreal summer and fall are the most conducive
614 to processes that encourage peaking of Niño-3 SSTA,
615 and prescribe the external forcing accordingly.

616 As mentioned above, all delays associated with lo-
617 cal coupling processes are assumed, for the sake of
618 simplicity, to be equal to β . We explore the region in
619 the parameter space that goes from a minimal value
620 of β (0.01 years) up to about 4 months (0.3 years).

621 In accordance with the broader view of the
622 delayed-oscillator concept adopted here, we allow the
623 “wave delay” τ that represents the ocean adjustment
624 time to vary from about 1 month in the fast-wave
625 limit [18,56,58] up to about 2 years. For reference
626 purposes, we recall that the calculated travel time
627 for the gravest Rossby wave mode is in the order of
628 one-and-a-half year [1].

629 4. Model solutions

630 We are now ready to present and discuss our BDE
631 model’s solutions, and compare their behavior with
632 that of other ENSO models. Numerical solutions were
633 obtained by the constructive algorithm presented in
634 Appendix A.1. This algorithm generalizes the one
635 of Dee and Ghil [28] to nonautonomous systems
636 of BDEs, like Eqs. (4)–(8) here. To avoid difficul-
637 ties with sensitivity of solutions to the ordering of
638 jump points in time, our numerical implementa-
639 tion relies on the object-oriented language C++: a
640 special class was created to represent real numbers
641 as strings of characters with arbitrary length (see
642 Appendix A.2).

4.1. Classification of solutions

643

644 Given the above initial data that describe a canon-
645 ical ENSO scenario [67] and plausible time delays,
646 we find that in the region where $\tau \geq \beta$, the BDE
647 system given by Eqs. (4)–(8) produces oscillatory
648 solutions with realistic periods. This is consistent
649 with the results of Schopf and Suarez [13] and Bat-
650 tisti and Hirst [14], as described in Section 3.1 here.
651 In the region $\tau < \beta$, the solutions are also oscil-
652 latory, but their periods are extremely short and
653 hence unrealistic. Almost all the solutions exhibit
654 initial transients. This numerical result confirms that
655 our BDE model for ENSO is dissipative, as sug-
656 gested by the presence of the dissipative Boolean
657 operators \wedge and \vee in Eqs. (6) and (8) (see Section
658 2.3).

659 The period P of a simple oscillatory solution is
660 defined here as the time between the onset of two
661 consecutive extreme warm events ($T_1 = T_2 = 1$ or
662 ENSO = 2). We use this definition to classify the
663 different solutions as follows.

664 4.1.1. Periodic solutions where the period
665 consists of a single cycle

666 In many cases, after the transients die down, the
667 solution settles into a simple periodic behavior. Over
668 whole τ -intervals, while the local delay β remains
669 fixed, what happens is that a simple cycle containing
670 one warm event followed by a cold one repeats itself.
671 For all such single-cycle solutions, the period is an
672 integer multiple of the seasonal cycle’s period, ϕ_f ,
673 taken equal to 1.0 (see Eq. (7)).

674 Each succession of events, or *internal cycle*, is
675 thus completely phase-locked to the seasonal cycle,
676 i.e., the warm events always peak at the same time
677 of year. The internal cycles follow the same sequence
678 of states—ENSO = $-2, 1, 2, -1$ (see Fig. 2)—
679 although the residence time within each state changes
680 as τ changes. At the lowest values of the wave delay
681 τ and coupled-processes delay β , such solutions have
682 the same periodicity as the forcing, i.e., 1 year. For
683 each fixed β , as τ is increased, intervals where the
684 solution has a simple period equal to 2, 3, 4, 5, 6, and
685 7 years arise consecutively. Clearly, for solutions of

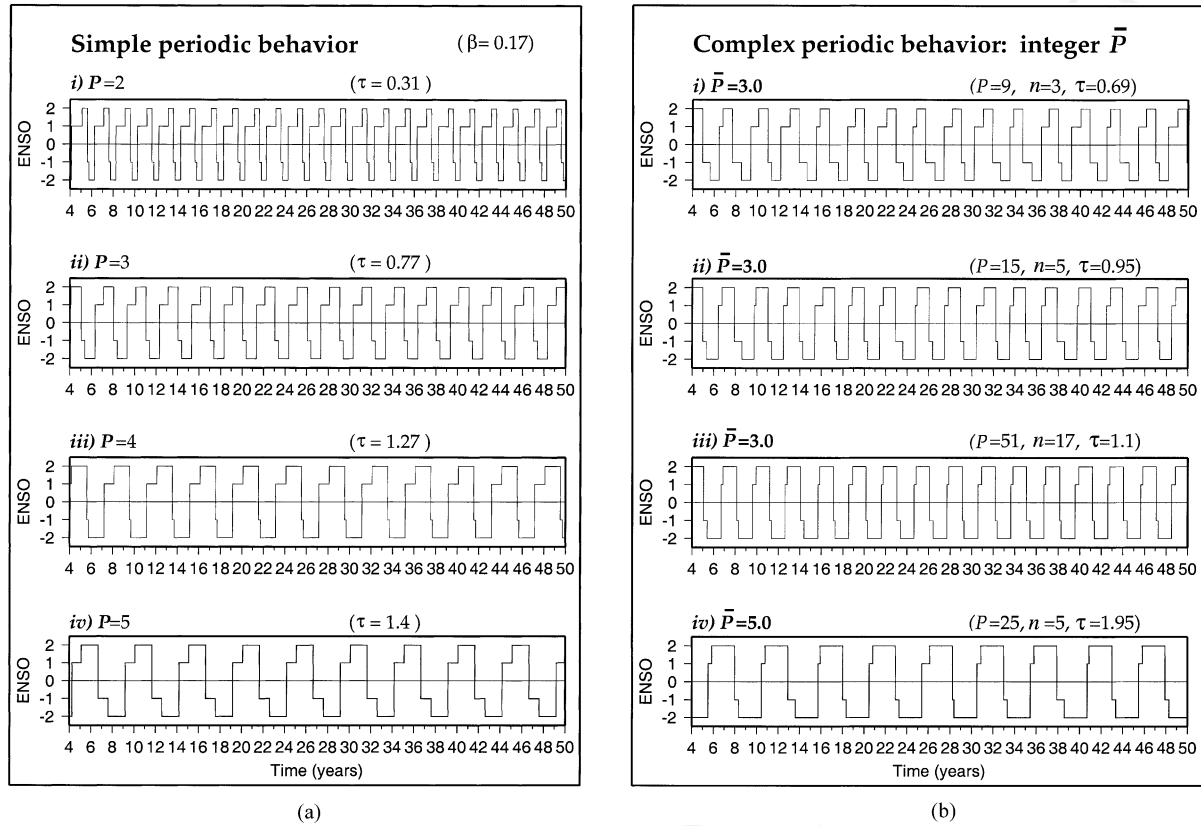


Fig. 2. The temporal evolution of BDE model solutions for a fixed local delay $\beta = 0.17$, and several wave-delay values τ , demonstrates the different types of behavior encountered. (a) Solutions that exhibit simple periodicity: after the transients die down, a cycle of a fixed integer-length period P repeats. Perfect phase-locking with the warming peak always taking place around the beginning of the calendar year. (i) $\tau = 0.31$, $P = 2$; (ii) $\tau = 0.77$, $P = 3$; (iii) $\tau = 1.27$, $P = 4$; (iv) $\tau = 1.4$, $P = 5$. (b) Solutions that exhibit more complex periodicity: a sequence of n cycles with different lengths repeats itself every P years. In these panels the average cycle length, $\bar{P} = P/n$, is an integer multiple of the annual cycle. The solutions are ordered according to the values of τ . (i) $\tau = 0.69$: the period is 9 years long and is comprised of $n = 3$ distinct cycles; (ii) $\tau = 0.95$: the period is 15 years long and is comprised of $n = 5$ cycles; (iii) $\tau = 1.1$: the period is 51 years and it is comprised of $n = 17$ cycles; (iv) $\tau = 1.952$: the period is 25 years long and is comprised of $n = 5$ cycles. The average cycle length is $\bar{P} = 3$ for panels (i)–(iii) and $\bar{P} = 5$ for panel (iv). (c) Solutions that exhibit complex periodicity and noninteger average period. A sequence of n different cycles repeats itself every P years; the average cycle length \bar{P} is now a *rational* rather than an *integer* multiple of the annual forcing period. (i) $\tau = 0.47$, $P = 5$ and $n = 2$; (ii) $\tau = 0.489$, $P = 67$ and $n = 29$; (iii) $\tau = 0.565$, $P = 22$ and $n = 9$; (iv) $\tau = 1.188334$, $P = 10$ and $n = 3$. (d) A sequence of different cycles unfolds, but no cyclical recurrence pattern is discerned during this finite computation: (i) $\tau = 0.474891$, $\bar{P} = 2.212907579 \dots$; (ii) $\tau = 0.519593782$, $\bar{P} = 2.4008526252 \dots$; (iii) $\tau = 0.53331$, $\bar{P} = 2.593307599 \dots$; (iv) $\tau = 0.579563$, $\bar{P} = 2.838877471 \dots$.

686 this type, P is a piecewise-constant, monotonically
687 nondecreasing function of τ .

688 In Fig. 2a, a few solutions with an integer period
689 of 2–5 years are presented for a fixed value of β and
690 increasing values of τ . The blue-colored dots in Fig. 3
691 represent points in the (τ, P) -plane where the solution
692 has such a simple, one-cycle integer period P ; these

points are organized as prominent plateaus at each
integer. 693
694

4.1.2. Periodic solutions where each period consists of several cycles 695 696

A slightly more complex type of behavior arises
in τ -intervals adjacent to the single-cycle ones. Se- 697
698

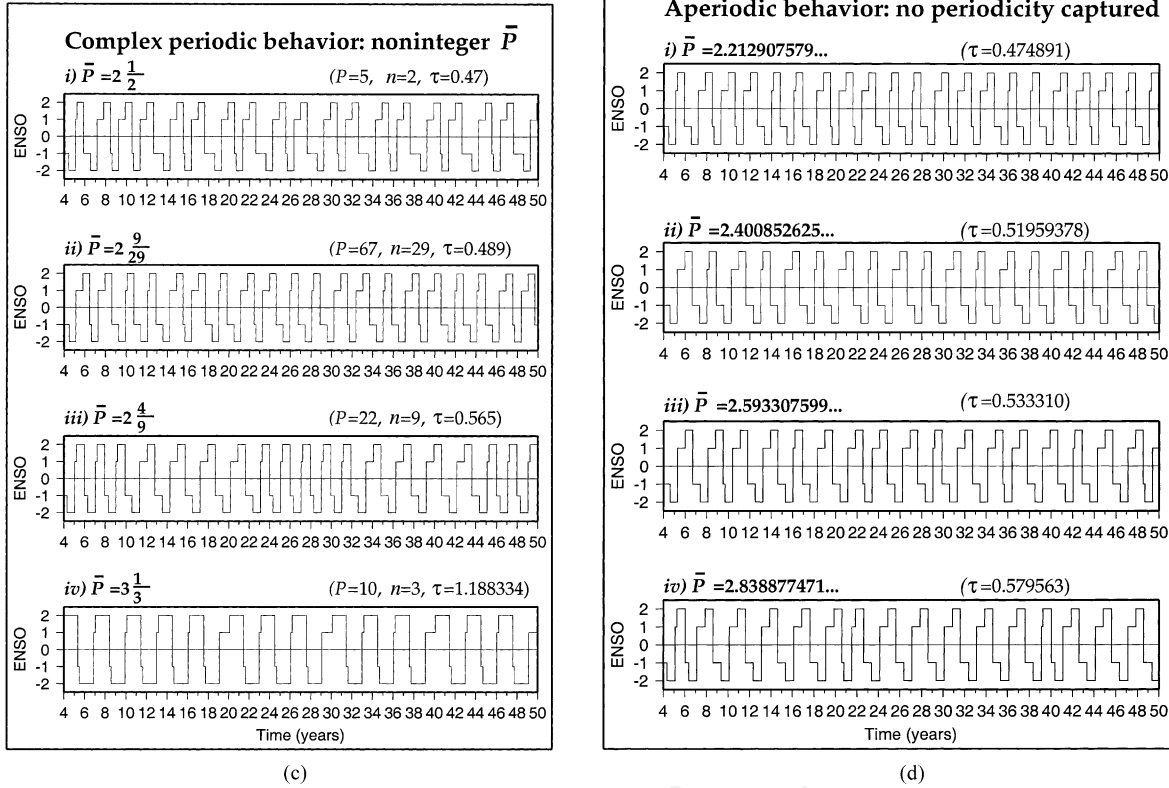


Fig. 2. (Continued).

699 quences of events with different temporal details un- 716
 700 fold and eventually repeat (Fig. 2b). As the finiteness 717
 701 of the number representation renders all delays ratio- 718
 702 nal, we do expect all computed solutions to be even- 719
 703 tually periodic. A pattern recognition algorithm was 720
 704 devised to identify sequences that repeat. Such a se- 721
 705 quence is assumed to be periodic after it has been ob- 722
 706 served to repeat more than a predetermined number 723
 707 of times. Once that is the case, we compute the aver- 724
 708 age length $\bar{P} = P/n$ of the cycles that the periodic 725
 709 sequence is comprised of; here P is the length of the 726
 710 sequence and n is the number of cycles. The solutions 727
 711 whose complete period is made up of several distinct 728
 712 internal cycles are shown as orange dots in Fig. 3. 729
 713 There are two types of composite-period solutions: 730

714 1. \bar{P} is an integer. Over substantial τ -intervals, av- 731
 715 erage cycle lengths that equal a constant integer 732

are still preferred. The length of the individual cy- 716
 717 cles that comprise the periodic sequence straddle 718
 719 the integer value of \bar{P} , as each cycle attempts to 720
 721 satisfy the phase-locking “inducement” built into 722
 722 Eq. (8). As τ is increased, combinations of cycles 723
 724 with lengths that are further and further removed 724
 725 from \bar{P} arise; their temporal details consequently 726
 726 feature weaker and weaker phase-locking (Fig. 2b). 727
 727 Then, at a certain τ -value, a threshold is crossed 728
 728 and a new average period \bar{P} , not necessarily an in- 729
 729 teger, is selected. 730

2. \bar{P} is a noninteger rational number. As the transi- 731
 732 tion from one broad step associated with an integer 732
 733 period to another occurs, \bar{P} is no longer an inte- 733
 733 ger, but instead a rational multiple of the annual 733
 733 period. As we transition from a period of 3 years 733
 733 to a period of 4 years (hereafter Region R3-4; see 733
 733 inset of Fig. 3), \bar{P} becomes a nondecreasing step 733

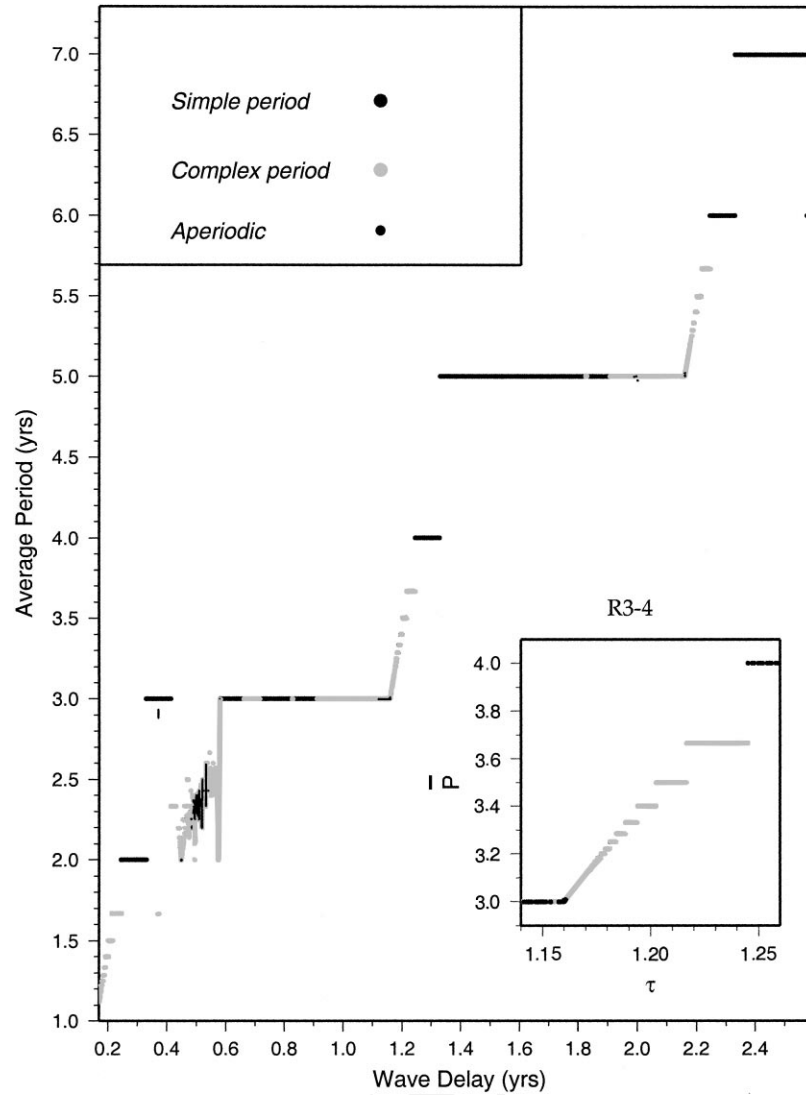


Fig. 3. The Devil’s staircase: a bifurcation diagram showing the average cycle length \bar{P} versus the wave delay τ for a fixed $\beta = 0.17$. Blue dots indicate purely periodic solutions, like those shown in Fig. 2a; orange dots are for complex periodic solutions, like those shown in Fig. 2b and c; small black dots denote aperiodic solutions, like in Fig. 2d. The inset shows a blow-up of the Devil’s staircase between periodicities of 3 and 4 years.

734 function of τ that takes only rational values, ar-
 735 ranged on a Devil’s staircase. The length of individ-
 736 ual cycles no longer straddles a single integer; in-
 737 stead, different combinations of values — bounded
 738 between the two bracketing integers — are chosen,
 739 while the individual cycles still “struggle” to re-
 740 main phase-locked (Fig. 2c). When all such ac-

ceptable sequences are exhausted, a jump to the 741
 next value of \bar{P} — a new *frequency-locking* step — 742
 occurs. 743

4.1.3. “Aperiodic” solutions 744

As explained above, we know that all the solutions 745
 that are generated by the time-marching algorithm de- 746

747 scribed in Appendix A.1 must be eventually periodic,
 748 as the only delays we can represent in this frame-
 749 work are rational. We did, however, encounter solu-
 750 tions with a period that was too long to be captured in
 751 our finite-length simulations. From BDE theory (see
 752 Section 2.3), we suspect that such solutions are ap-
 753 proximations to solutions of the system for irrational
 754 delays that may be QP or aperiodic. For such points,
 755 we define $\bar{P} = \bar{P}(\tau)$ to be the simple average of cycle
 756 length over the whole simulation performed for that
 757 delay value τ . The corresponding points are plotted in
 758 black in Fig. 3, and complement the picture portrayed

759 by points of type Sections 4.1.1 and 4.1.2 that are
 760 more frequently encountered in our phase-parameter
 761 space.

4.2. The “classic” QP route to chaos in the BDE model 762 763

The frequency-locking behavior observed for our
 764 BDE solutions above is a signature of the universal
 765 QP route to chaos. Its mathematical prototype is the
 766 Arnol’d circle map [33], given by the equation 767

$$\theta_{n+1} = \theta_n + \Omega + 2\pi K \sin(2\pi \theta_n) \text{ mod } 1. \quad (9) \quad 768$$

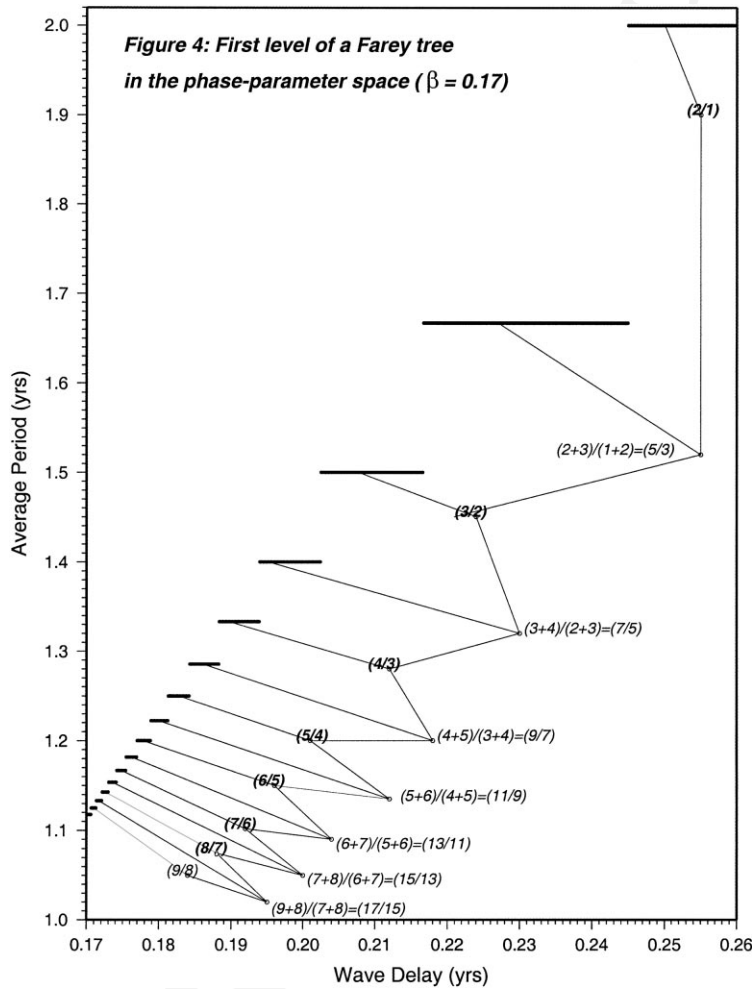


Fig. 4. The first level of Farey-tree ordering as revealed in our model results in the transition region between the periods of 1 and 2 years; $\beta = 0.17$. The widest step between two rationals p/q and r/s corresponds to $(p+r)/(q+s)$.

769 Eq. (9) describes the motion of a point denoted by
 770 the angle of its location on a unit circle that under-
 771 goes repeated shifts by a fixed angle along the circle’s
 772 circumference. The point is also subject to nonlinear
 773 sinusoidal “corrections,” with the size of the nonlin-
 774 earity controlled by a parameter K .

775 We look at the winding number $\omega = \omega(\Omega, K) =$
 776 $\lim_{n \rightarrow \infty} [(\theta_n - \theta_0)/n]$, which can be described roughly
 777 as the average shift of the point per iteration. When the
 778 nonlinearity’s influence is small, this average shift —
 779 and hence the average period — is determined largely
 780 by Ω ; it may be rational or irrational, with the latter

781 being more probable due to the irrationals’ pervasiv-
 782 ness. As the nonlinearity K is increased, “Arnol’d
 783 tongues” — where the winding number ω locks to
 784 a constant rational over whole intervals — form and
 785 widen. At a critical parameter value, only rational
 786 winding numbers are left and a complete Devil’s
 787 staircase crystallizes. Beyond this value, chaos reigns
 788 as the system jumps irregularly between resonances
 789 [68,69].

790 The average cycle length \bar{P} defined for our ENSO
 791 system of BDEs is clearly analogous to the circle
 792 map’s winding number in both its definition and

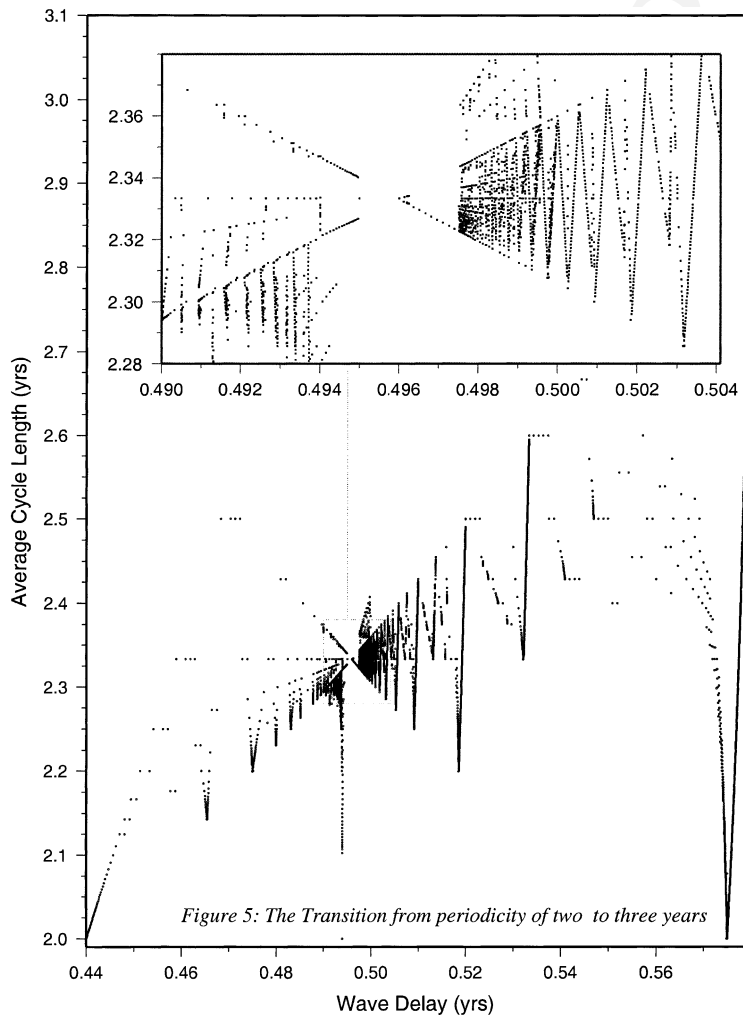


Fig. 5. A blow-up of the transition zone from average periodicity 2–3 years; $\tau = 0.4\text{--}0.58$, $\beta = 0.17$. The inset is a zoom on $0.49 \leq \tau \leq 0.504$. A complex mini-staircase structure reveals self-similar features, with a focal point at $\tau \approx 0.5$.

793 behavior. The transition to chaos along this route
 794 [70] depends on the two parameters Ω and K ,
 795 which determine the approximate period and de-
 796 gree of irregularity of the system’s behavior, respec-
 797 tively.

798 A closer look at the unfolding of the route to chaos
 799 in our BDE model (Fig. 3) shows that most transition
 800 zones resemble region R3-4 in exhibiting “orderly”
 801 Devil’s meso-staircases, or “ladders”. The fractional
 802 parts of the averaged periodicities \bar{P} in each ladder are
 803 arranged in a Farey tree ordering (see Fig. 4) where
 804 the widest step between two rationals, p/q and r/s ,
 805 corresponds to $(p + r)/(q + s)$. This Farey tree or-

806 dering of the “stairs” of a Devil’s staircase is another
 807 signature of the QP scenario [68,69].

808 The jumps between steps are densely clustered near
 809 the bottom of each ladder, while the steps grow broader
 810 and further apart as the system ascends towards the
 811 next integer period. Our numerous and systematic, but
 812 still *finite*, computations indicate that some intermedi-
 813 ate steps might be skipped altogether or are so minute
 814 as not to be resolved by our discrete sampling of τ ;
 815 this suggests that the system is below criticality, in this
 816 τ -interval, for the given β -value.

817 Several physical systems — such as the periodically
 818 forced pendulum, Josephson junctions, and Ising mod-

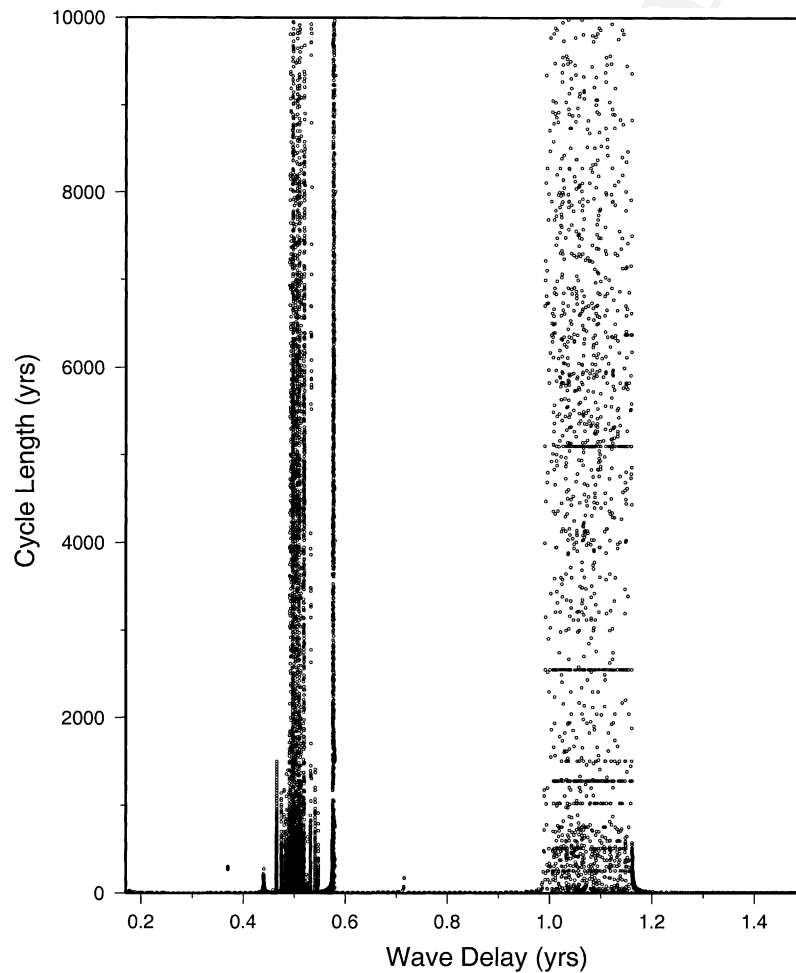


Fig. 6. A plot of the unaveraged period length P versus τ . The high-density strips around $\tau \approx 0.5$ and $\tau = 1$ exhibit numerous points where finite-length computations did not capture a recurring sequence of cycles of finite period.

819 els [71,72]—exhibit this QP route to chaos as their
 820 nonlinearity is increased. Its relevance to ENSO dy-
 821 namics has been previously demonstrated by Chang
 822 et al. [60,61], Jin et al. [30,62], and Tziperman et al.
 823 [63,64]. We will discuss the connection between the
 824 results of these authors using differentiable dynamical
 825 systems and ours using BDEs in Section 5.

826 4.3. The fractal sunburst—a “bizarre attractor”

827 A much more complex, and heretofore unsuspected,
 828 “fractal sunburst” structure emerges as the system
 829 undergoes the transition from an averaged period of
 830 2–3 years (Fig. 5). As the wave delay τ is increased,
 831 mini-ladders build up, collapse or descend, only to
 832 start climbing up again. The pattern’s focal point
 833 occurs near a critical value of $\tau \cong 0.5$ years. In the
 834 vicinity of this focal point, the mini-ladders rapidly
 835 condense and the structure becomes self-similar,
 836 with each zoom revealing the pattern repeated on a

837 smaller scale. The sequences of events in the cor-
 838 responding solutions become increasingly complex
 839 and require longer and longer computations before
 840 repetition is captured (Fig. 6). Within this fractal
 841 sunburst pattern, when repetition does eventually oc-
 842 cur, the average periodicity \bar{P} is always between 2
 843 and 3.

844 As previously stated (see Section 2.3), all the so-
 845 lutions that are numerically computed are *eventually*
 846 *periodic*. Theoretical results [29] indicate, however,
 847 that truly aperiodic solutions for irrational delays—
 848 in the neighborhood of this critical delay value—are
 849 being approximated by such long-periodic solutions.
 850 The mechanism by which aperiodicity is generated, in
 851 our BDE framework, is due to a clustering of solution
 852 jump points in a given time interval. Slight changes
 853 in delay values (or alternatively initial data) cause re-
 854 ordering of these jump points, thus enabling different
 855 feedbacks to take precedence and change the solution
 856 qualitatively.

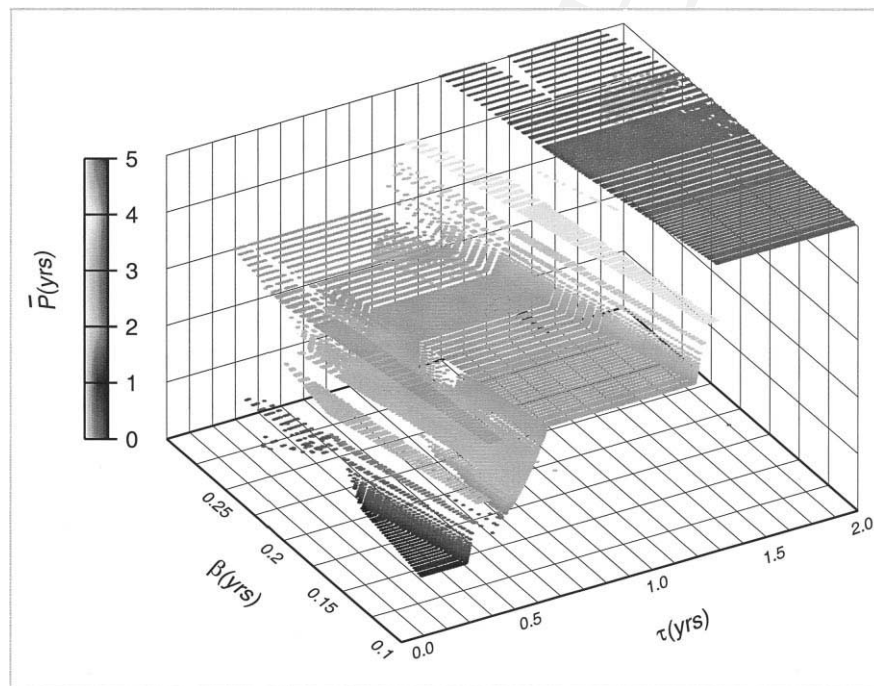


Fig. 7. The Devil’s bleachers: a three-dimensional regime diagram showing the average cycle length \bar{P} , portrayed in both height and color, versus the two delays β and τ . Oscillations are produced even for very small values of β , as long as $\beta \leq \tau$. Variations in τ determine the oscillation’s period, while changing β establishes the bottom step of the staircase, shifts the location of the steps, and determines their width.

857 The fractal sunburst pattern found here in the BDE
 858 system’s phase-parameter space could be dubbed a
 859 “bizarre attractor” for lack of a better word. It bears
 860 a loose analogy to the “strange attractor” seen in the
 861 phase space of dissipative ODEs. This is the first de-
 862 scription, to the best of our knowledge, of the ability
 863 of BDE systems to capture complex behavior on the
 864 “edge of chaos”. The presence of such a bizarre at-
 865 tractor between periods 2 and 3 suggests a heretofore
 866 unexplored mechanism that affects the irregularity of
 867 ENSO occurrences and, more particularly, the width
 868 of the quasi-biennial, 2–3-year peak of ENSO vari-
 869 ability.

870 The influence of the local-processes delay β , along
 871 with that of the wave-dynamics delay τ , is shown in
 872 the three-dimensional “Devil’s bleachers” (or “Devil’s
 873 terrace” according to Jin et al. [30]) of Fig. 7. We
 874 see that oscillations are produced even for very small
 875 values of β , as long as $\beta \leq \tau$.

876 While our model ventures away from the classic
 877 Devil’s staircase associated with the QP route to chaos,
 878 Fig. 8 provides finer fingerprints as evidence that the
 879 scenario is still relevant. In this figure, we plot the
 880 step widths that are associated with each rational value
 881 p/q of the average cycle length \bar{P} . The emerging
 882 self-similar pattern bears a striking resemblance to

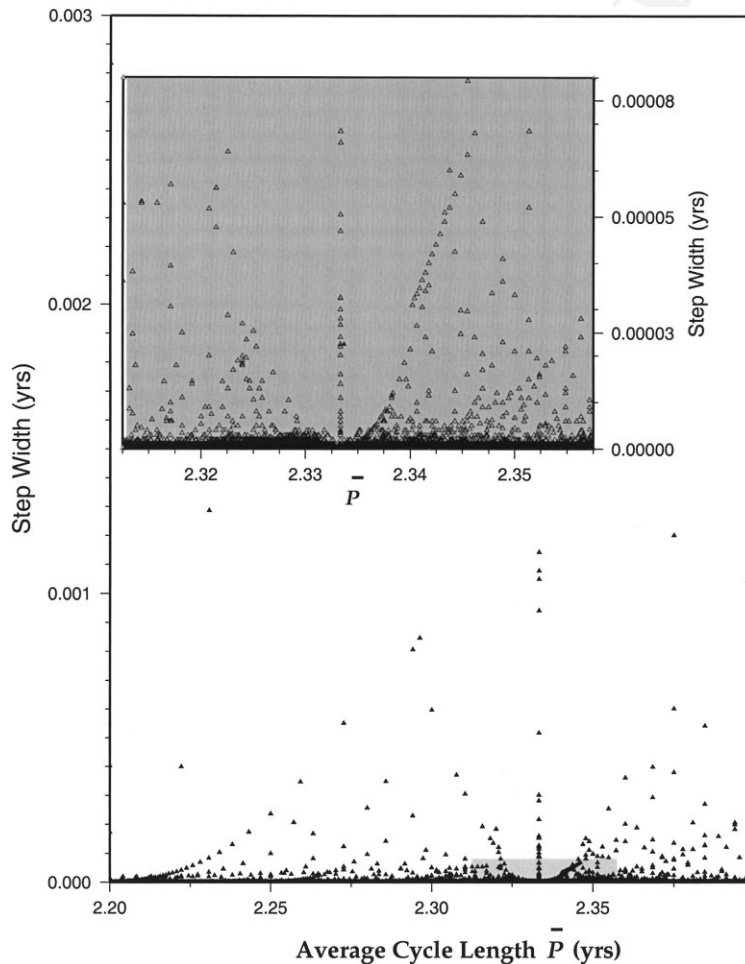


Fig. 8. Devil’s-staircase step widths associated with each average cycle length \bar{P} , for $2.2 \leq \bar{P} \leq 2.4$. The inset shows a zoom of the small gray rectangular area, $2.3125 \leq \bar{P} \leq 2.3575$, and highlights the self-similar nature of the pattern.

883 the one obtained when plotting step widths associated
 884 with the winding numbers for the circle map and for
 885 Josephson junctions [72]. In this particular τ -interval,
 886 our system is clearly just above criticality as it jumps
 887 in an erratic yet structured manner between competing
 888 frequencies.

889 5. Summary and discussion

890 5.1. Summary of results

891 In this study, we have used the modeling frame-
 892 work of BDEs to formulate a highly idealized ENSO
 893 model that embodies the critical elements of the
 894 delayed-oscillator concept and its interaction with
 895 the annual cycle. Our semi-discrete BDE model is
 896 comprised of continuous-time evolution equations
 897 in terms of logical operations on discrete variables
 898 (see Table 1). Internal variables that describe the
 899 oceanic and atmospheric anomalies have four levels
 900 each, with the extreme values designating El Niño or
 901 La Niña conditions, respectively, while an external
 902 seasonal-forcing variable has two levels (see Fig. 1a).
 903 The BDE framework has thus been extended to in-
 904 clude: (i) the possibility of *multi-level* variables when
 905 more than two states are necessary, while retaining the
 906 simplicity of a few discrete levels; and (ii) modeling
 907 of *periodically forced* dynamical systems in addition
 908 to *autonomous* systems.

909 In spite of its extreme simplicity, our BDE model
 910 displays a wealth of temporal behavior that captures
 911 key features apparent in more traditional models based
 912 on PDEs, DDEs or FDEs. It also reveals a complex
 913 “bizarre attractor” that takes the form of a “fractal
 914 sunburst” in the model’s phase-parameter space. This
 915 behavior was not observed before, to the best of our
 916 knowledge, in any type of dynamical system. In the
 917 ENSO application at hand, it may provide a clue to
 918 the irregularity revealed by the observational data, in
 919 general, and to the width of the quasi-biennial peak,
 920 in particular.

921 A puzzling gap that had existed in BDE theory
 922 is bridged by the discovery of this bizarre attrac-
 923 tor. The only solutions obtained so far were either

924 completely regular—constant or periodic—or ex-
 925 hibited a power-law growth in complexity. This study
 926 provides the first evidence of BDEs capturing “or-
 927 der on the edge of chaos” behavior, with bounded,
 928 rather than growing complexity. This type of be-
 929 havior is illustrated here by the universal QP route
 930 to chaos. This route is present in our model in its
 931 classic form of the Devil’s staircase, as well as in
 932 the more complex, self-similar version of the fractal
 933 sunburst.

934 5.2. Physical interpretation

935 In the context of ENSO theory, the results obtained
 936 from our minimal model reinforce the view that the in-
 937 teraction between the inherent ENSO oscillator and the
 938 seasonal cycle plays a significant dual role in ENSO
 939 dynamics. According to this view, the interaction in-
 940 troduces a degree of regularity by modifying the pe-
 941 riod length to accommodate the preference for sea-
 942 sonal phase locking. It also introduces irregularity, as
 943 a result of a low-order, deterministically chaotic pro-
 944 cess. In this section, we place our results in the context
 945 of other models and data analyses that support this
 946 view. We also mention studies that attribute ENSO’s
 947 irregularity to other effects and discuss briefly their
 948 relative merits. A more detailed comparative discus-
 949 sion of ENSO theories can be found in Neelin et al.
 950 [9,20] and Ghil and Robertson [10].

951 Tziperman et al. [63] have added a sinusoidal forc-
 952 ing term to a differential-delay “toy model” similar to
 953 Eq. (3). As the coupling strength between atmospheric
 954 and oceanic effects is increased, the system progresses
 955 from complete frequency locking to the seasonal cy-
 956 cle, through having a few dominant spectral peaks
 957 (with no apparent frequency locking), and on to a
 958 frequency-locked quasi-quadrennial regime. For even
 959 larger values of the coupling parameter chaos reigns,
 960 as the model leaps between different “overlapping”
 961 resonances.

962 Jin et al. [30,62] have added a *prescribed* annual cy-
 963 cle to a more realistic yet still *simple model* [18,56,58],
 964 based on a stripped-down version of the Cane and Ze-
 965 biak [16] model. Their model shows a prevalence of
 966 subcritical frequency-locking regimes in its parame-

967 ter space, with Devil’s staircase signatures in narrow
968 transition regions between integer periodicities.

969 Chang et al. [60] constructed a more sophisticated
970 *intermediate* coupled model that could develop its
971 own seasonal cycle. As the forcing amplitude is in-
972 creased, the model’s initially stable 40-month oscil-
973 lation undergoes “period-doubling” bifurcations. For
974 even higher values of the forcing frequency locking
975 is achieved. At a realistic forcing level, their model’s
976 ENSO cycle falls into its most chaotic regime. This oc-
977 curs in the same frequency band in which the “bizarre
978 attractor” is located in our BDE model.

979 Low-order chaotic processes are also sometimes de-
980 tected via calculations of geometric phase-space di-
981 mensions. To perform such calculations on the obser-
982 vational data would be meaningless, given the short-
983 ness — only about a 100 years — of the instrumental
984 record (see Ghil et al. [73] and references therein).
985 Chang et al. [60] and Tziperman et al. [63] have calcu-
986 lated, however, these dimensions in their much longer
987 models’ simulations, while verifying that the latter can
988 be distinguished reliably from purely random “surro-
989 gate data”. They have arrived at fractal dimensions of
990 5.2 and 3.5, in their respective models, both of which
991 indicate low-dimensional deterministic chaos.

992 Finally, spectral analyses of the time series of var-
993 ious ENSO-related *observed* quantities cannot yield
994 conclusive evidence on the mechanisms for ENSO
995 regularity and irregularity, due again to the shortness
996 of the record. A number of significant pointers do
997 arise, however. First, classical power spectrum anal-
998 ysis indicates a broad peak around 3–5 years super-
999 imposed on a broad-band background [67]. Second,
1000 Rasmusson et al. [24] have analyzed the Compre-
1001 hensive Ocean Atmosphere Data Set (COADS) for
1002 the Indo-Pacific basin using single-channel SSA — a
1003 data-adaptive technique that is especially suited for
1004 short and noisy time series [74] — and found a sepa-
1005 rate quasi-biennial peak, as well as a lower-frequency
1006 one between 4 and 5 years. Third, Jiang et al. [25]
1007 applied a multi-channel version of SSA [75] to
1008 COADS data for 1950–1990 over the tropical Pa-
1009 cific and separated a quasi-biennial peak, a sharper
1010 quasi-quadrennial peak, and yet another one that cor-
1011 responds to a $(\frac{4}{3})$ -year periodicity. The existence of

the $(\frac{4}{3})$ -peak is consistent with the QP route to chaos, 1012
as it completes the sequence of periodicities $\frac{4}{1}$, $\frac{4}{2}$, $\frac{4}{3}$ 1013
and $\frac{4}{4}$ years exhibited clearly by Jin et al. [30,62] and 1014
our BDE model. 1015

The model results and data analyses reviewed herein 1016
thus support the hypothesis that the interaction of the 1017
annual cycle with the ENSO oscillator sends the sys- 1018
tem on the QP route to chaos [9,10]. This determinis- 1019
tic chaos then causes the observed irregularity, evident 1020
in the broad spectral background. The observational 1021
analyses also help reject the “period-doubling” scen- 1022
ario as a culprit, since it would entail a quasi-biennial 1023
peak that is more prominent than the quasi-quadrennial 1024
peak, while the observations exhibit the opposite [25]. 1025

The most important alternative hypothesis attributes 1026
the cause of ENSO irregularity to stochastic weather 1027
“noise”, such as westerly wind bursts over the cen- 1028
tral Pacific, with decorrelation times that are short in 1029
comparison with other ENSO timescales [76,77]. The 1030
relative importance of weather noise versus determin- 1031
istically chaotic dynamics is an actively debated topic 1032
[78,79]. At present, most detailed three-dimensional 1033
deterministic models show a strong preference for peri- 1034
odic or QP behavior, thus failing to explain the ir- 1035
regularity evident in the observations. Linear stochas- 1036
tically driven models, on the other hand, do not cap- 1037
ture many of the observed features of ENSO variabil- 1038
ity, in particular, the tendency for phase locking to 1039
the boreal winter. Stochastically perturbed *nonlinear* 1040
models, however, seem to be more successful and may 1041
provide a possible synthesis of the two approaches 1042
[30,78]. 1043

High-frequency stochastic processes, as well as 1044
low-frequency deterministic processes on the time 1045
scale of decades [80,81] may provide explanations 1046
for two questions whose importance is highlighted 1047
and yet unanswered by the above simple models: 1048
(i) how are the relevant parameter regions, i.e., the 1049
oceanic and atmospheric response time scales, for 1050
the observed phenomena selected?; and (ii) what are 1051
the processes that are responsible for the apparent 1052
substantial shifts in their values over time? 1053

For example, Ghil and Jiang [31] and Kirtman 1054
and Schopf [82] independently, argued that the 1055
delayed-oscillator mechanism has “failed” in the 1056

1057 1990s and that this failure lead to: (a) the long
 1058 mild event that lasted from 1990 to 1995 and
 1059 (b) the resulting diminished predictive skill of all
 1060 ENSO-prediction models, relative to the preceding
 1061 decade. In the framework of the simple delay differ-
 1062 ential and BDE models discussed so far, this change
 1063 corresponds to the system shifting into a parame-
 1064 ter range where local processes are boosted relative
 1065 to the oceanic ones, so that the interannual oscil-
 1066 lations are not sustained. More light may be shed
 1067 on the validity and dynamical causes of such shifts
 1068 in the parameter space by currently active research
 1069 that focuses on the following areas: the role of ad-
 1070 ditional feedbacks not previously modeled, e.g., the
 1071 evaporative–convective feedback [83]; interaction
 1072 with other tropical, but intraseasonal or seasonal phe-
 1073 nomena such as the Madden-Julian oscillation [84]
 1074 and the Indian monsoon [85,86]; and interdecadal
 1075 variations due to interaction with the extratropical
 1076 oceans [87].

1077 ENSO studies will undoubtedly continue to be nour-
 1078 ished by the interplay between models that range from
 1079 highly detailed to very simple ones [10]. It is our hope
 1080 that BDEs will prove to be a useful tool for prelimi-
 1081 nary theoretical studies in this model hierarchy. In ad-
 1082 dition, the focus in ENSO and other climate studies
 1083 is shifting to interdecadal variations and even longer
 1084 time scales that involve ever more subsystems, pro-
 1085 cesses, and feedbacks. We expect nontraditional tools
 1086 such as the one presented here to play an increasingly
 1087 important role in studying the complex systems that
 1088 are the object of these investigations.

1089 Acknowledgements

1090 We would like to thank Drs. David Neelin and Fer-
 1091 enc Varadi for helpful discussions. Bill Weibel and
 1092 Dr. Juan Restrepo assisted generously with the plots,
 1093 while Françoise Fleuriau helped with word processing
 1094 and the bibliography. The plots were generated by the
 1095 Generic Mapping Tools [88]. Our research was sup-
 1096 ported by NSF grant ATM00-82131. This is publica-
 1097 tion number 5651 of UCLA’s Institute of Geophysics
 1098 and Planetary Physics.

Appendix A. Numerical formulation of the BDE system 1099 1100

A.1. The algorithm 1101

A constructive algorithm yields the time-marching 1102 solution to the periodically forced BDE system 1103 (4)–(8). The algorithm is an extension of the algorithm 1104 first formulated by Dee and Ghil [28] for *autonomous* 1105 systems and it permits the construction of solutions 1106 for *periodically forced* systems as well. 1107

To construct a solution, it is required that admissi- 1108 ble initial data be supplied over a time-interval whose 1109 length $b - a$ is greater or equal to the maximal de- 1110 lay value allowed $\bar{\theta}_{\max}$. Admissible initial data are 1111 piecewise-constant, i.e., there are only a finite num- 1112 ber of points where one or more of the Boolean state 1113 variables x_i , $1 \leq i \leq n$, may “jump” from 0 to 1 or 1114 vice-versa. 1115

A.1.1. Initialization step ($N = 0$) 1116

At first, we construct a set M_0 that represents the ini- 1117 tial data, or “memory” of the system. Each element in 1118 M_0 is an ordered pair, $p_k = (t_k, \vec{x}_k)$ with $0 \leq k \leq m$. 1119 The right coordinate is a time point, or *epoch* t_k that is 1120 the left-end point of a maximal subinterval $[t_k, t_{k+1}) \subseteq$ 1121 $[a, b)$ over which all of the system’s Boolean vari- 1122 ables remain constant. The left coordinate is a Boolean 1123 vector $\vec{x}_k(t_k) = (x_1(t_k), x_2(t_k), \dots, x_n(t_k)) \in \mathcal{B}^n$ that 1124 holds the constant values of the variables over the 1125 subinterval $[t_k, t_{k+1})$. The elements $p_k = (t_k, \vec{x}_k)$ in 1126 the set M_0 are ordered so that their epochs are in 1127 ascending order: $a \leq t_1 \leq \dots \leq t_{m-1} \leq t_m \leq b$. 1128

Next, we create a set P_0 that contains all *potential* 1129 future jump points of the system’s variables, where 1130 the equations will have to be solved. In addition to the 1131 upper bound of the initial interval, more epochs are 1132 added according to the following criteria: (a) assume 1133 an *internal* variable x_j has jumped at time t_k . For 1134 every variable x_i that depends on past values of x_j at 1135 $t - \theta_{i,j}$, add a possible jump point $t_k + \theta_{i,j}$ to P_0 ; (b) 1136 if an *external* variable “jumped” at an epoch t_l and 1137 ϕ_f is the forcing period associated with that variable, 1138 add $t_l + \phi_f$ to P_0 . Naturally, P_0 is also arranged in an 1139 ascending order. 1140

1141 A.1.2. *General step* ($N = 1, 2, \dots$)

1142 After the completion of step N , the set M_N holds the
1143 relevant *past* memory of the system, while the set P_N
1144 contains its potential *future* jump points. The solution
1145 is then advanced in time as follows.

1146 Let t_N^* be the first epoch in P_N . The evolution equa-
1147 tions are used to evaluate the values of all state vari-
1148 ables at that epoch. To achieve that, the pertinent in-
1149 formation from the “past” has to be retrieved from the
1150 “memory” M_N . Specifically, to evaluate $x_i(t_N^*)$, one
1151 has to determine the value of $x_j(t_N^* - \theta_{i,j})$ for all state
1152 variables x_j and delays $\theta_{i,j}$ that appear in the i th ev-
1153 olution equation. This is done using a search algorithm
1154 that returns the element $p_k = (t_k, \vec{x}_k) \in M_N$ whose
1155 epoch t_k is the largest one that is smaller than or equal
1156 to the targeted epoch $t_N^* - \theta_{i,j}$. The values extracted
1157 are then substituted into the evolution equations and
1158 the Boolean expressions are evaluated. A new element
1159 $p_N^* = (t_N^*, \vec{x}_N^*)$ that consists of the time epoch to-
1160 gether with the newly determined state vector $\vec{x}_N^*(t_N^*)$
1161 is added to the solution and to M_N as we begin form-
1162 ing the new relevant *memory* set M_{N+1} .

1163 The memory is further updated as we remove a
1164 subset D_N of M_N that contains the elements no longer
1165 needed, since they now lie outside the “memory span”
1166 of length θ_{\max} used to resolve the system’s “future”,
1167 where $\theta_{\max} \leq \hat{\theta}_{\max}$ is the maximal delay value for
1168 the specific case solved. We do so by discarding all
1169 elements $p = (t, x)$ such that there exists another
1170 element $\hat{p} = (\hat{t}, \hat{x}) \in P_N$, for which $t \leq \hat{t} \leq (t_N^* -$
1171 $\theta_{\max})$. The newly updated memory set is $M_{N+1} =$
1172 $M_N \cup \{p_N^* = (t_N^*, \vec{x}_N^*)\} - D_N$.

1173 Finally, a new “future set” P_{N+1} is constructed.
1174 First, the newly resolved epoch t_N^* is removed from
1175 P_N . Then, new epochs are added according to essen-
1176 tially the same rules used in the construction of P_0 in
1177 the initialization step: (a) if an *internal* variable x_j has
1178 jumped at time t_N^* , then for every variable x_i that de-
1179 pends on past values of x_j at $t - \theta_{i,j}$, we add a possible
1180 jump point, $t = t_N^* + \theta_{i,j}$; (b) if an *external* variable x_f
1181 jumped at the epoch t_N^* , we add $t = t_N^* + \phi_f$ to P_{N+1} .
1182 These rules dictate, in effect, a more passive role for
1183 the forcing variables than that of internal variables.
1184 When an internal variable jumps, it “*communicates*”
1185 with the other variables by introducing all new future

epochs, where that change may affect them. External 1186
variables, on the other hand, contribute only epochs 1187
where their own value, that is never affected by the 1188
internal variables, may change. 1189

A solution can thus be continued for any desired 1190
length of time. For the ENSO model developed in Sec- 1191
tion 3, there is a unique forcing period, $\phi_f = 1$, while 1192
 $\theta_{\max} = \max\{\beta, \tau, 1\}$. The jumps in the periodic forc- 1193
ing guarantee in our case that the set P_N of potential 1194
future jump points for this specific system is never 1195
empty. 1196

A.1.3. *Numerical implementation* 1197

At any step N of solving the BDE system, it is not 1198
known how many points may be contained in either 1199
the system’s memory M_N or in its immediate future 1200
 P_N . Ghil and Mullhaupt [29] have shown the existence 1201
of BDE systems that exhibit polynomially growing 1202
complexity, as indicated by a power-law growth of the 1203
number of jumps per unit time. Thus the natural choice 1204
is to use dynamic memory allocation and implement 1205
the ordered sets M_N and P_N as linked lists. 1206

The solutions are known to be sensitive to the order- 1207
ing of jump points. As their numerical computation 1208
involves numerous additions of small numbers (the 1209
delays), it is prone therewith to cumulative round-off 1210
errors. Moreover, a solution to a system may include 1211
jump points that are so close, that they would be con- 1212
sidered equal in floating-point representation, which 1213
may result in a qualitative change in the solution’s be- 1214
havior. Therefore, we have carried out the computa- 1215
tions using an exact representation of the real numbers, 1216
rather than their usual floating-point representation. 1217
This was achieved by writing the code in C++, an 1218
object-oriented language, and creating a special class 1219
where real numbers are represented as strings of char- 1220
acters. Arithmetic operations are performed on objects 1221
of this class essentially as they would be by hand and 1222
are exact, as long as only finite strings are used. 1223

Two other viable representations of real numbers 1224
for computations of BDE solutions are the following: 1225
(i) a rational-number class — as all numbers repre- 1226
sentable on a finite computer are rational, each num- 1227
ber may be stored as a pair of integers corresponding 1228
to the denominator and numerator, with operations de- 1229

1230 fined accordingly; (ii) an interval-number class — each
 1231 floating-point number x represents $x \pm \epsilon$, where ϵ is
 1232 the accuracy desired [89]. The former representation
 1233 may be useful if one wishes to approximate irrational
 1234 numbers by using, e.g., continued fractions (see the
 1235 approximation theorem in Section 2.3 here and Ghil
 1236 and Mullhaupt's [29] use of these to approximate irra-
 1237 tional delays). The latter will render the computations
 1238 more rapid and require less memory, when exactness
 1239 of the solution is less crucial.

1240 We have chosen the string-representation approach
 1241 as it allows exact computations, while being signifi-
 1242 cantly more efficient than the quotient-representation
 1243 class. Another advantage of our approach is that we are
 1244 not restricted by the bounds on integers representable
 1245 on the specific machine used if we wish to carry out
 1246 computations at very high resolution in the system's
 1247 parameter space. Moreover, in an object-oriented lan-
 1248 guage like C++, a particular class can easily be re-
 1249 placed by any other class representing real numbers
 1250 and their operations, without changing the implemen-
 1251 tation of the actual solution algorithm.

1252 References

- 1253 [1] S.G.H. Philander, El Niño, La Niña, and the Southern
 1254 Oscillation, Academic Press, San Diego, 1990.
- 1255 [2] H.F. Diaz, V. Markgraf (Eds.), El Niño: Historical and
 1256 Paleoclimatic Aspects of the Southern Oscillation, Cambridge
 1257 University Press, New York, 1992.
- 1258 [3] K. Wyrtki, Water displacements in the Pacific and the genesis
 1259 of El Niño cycles, *J. Geophys. Res.* 90 (1985) 7129–7132.
- 1260 [4] D.E. Harrison, N.K. Larkin, Three COADS sea level pressure
 1261 signals: a near-global El Niño composite and time-series view,
 1262 1946–1993, *J. Clim.* 9 (1996) 3025–3055.
- 1263 [5] M.H. Glantz, R.W. Katz, N. Nicholls (Eds.), Teleconnections
 1264 Linking Worldwide Climate Anomalies: Scientific Basis and
 1265 Societal Impact, Cambridge University Press, New York,
 1266 1991.
- 1267 [6] T.C. Piechota, J.A. Dracup, Drought and regional hydrologic
 1268 variation in the United States: associations with the El Niño,
 1269 *Water Resour. Res.* 32 (1996) 1359–1373.
- 1270 [7] M. Latif, T.P. Barnett, M. Flügel, N.E. Graham, J.-S. Xu, S.E.
 1271 Zebiak, A review of ENSO prediction studies, *Clim. Dyn.* 9
 1272 (1994) 167–179.
- 1273 [8] J. Bjerknes, Atmospheric teleconnections from the equatorial
 1274 Pacific, *Mon. Wea. Rev.* 97 (1969) 163–172.
- 1275 [9] J.D. Neelin, M. Latif, F.-F. Jin, Dynamics of coupled
 1276 ocean–atmosphere models: the tropical problem, *Annu. Rev.*
 1277 *Fluid Mech.* 26 (1994) 617–659.
- [10] M. Ghil, A.W. Robertson, Solving problems with GCMs: 1278
 general circulation models and their role in the climate 1279
 modeling hierarchy, in: D. Randall (Ed.), *General Circulation* 1280
Model Development: Past, Present and Future, Academic 1281
 Press, New York, 2000, pp. 285–325. 1282
- [11] J.D. Neelin, M. Latif, M.A.F. Allaart, M.A. Cane, U. Cubasch, 1283
 W.L. Gates, P.R. Gent, M. Ghil, C. Gordon, N.C. Lau, C.R. 1284
 Mechoso, G. Meehl, J.M. Oberhuber, S.G.H. Philander, P.S. 1285
 Schopf, K.R. Sperber, A. Sterl, T. Tokioka, J.J. Tribbia, S.E. 1286
 Zebiak, Tropical air–sea interaction in general circulation 1287
 models, *Clim. Dyn.* 7 (1992) 73–104. 1288
- [12] C.R. Mechoso, A.W. Robertson, N. Barth, M.K. Davey, P. 1289
 Delecluse, P.R. Gent, S. Ineson, B. Kirtman, M. Latif, H. Le 1290
 Treut, T. Nagai, J.D. Neelin, S.G.H. Philander, J. Polcher, 1291
 P.S. Schopf, T. Stockdale, M.J. Suarez, L. Terry, O. Thual, 1292
 J.J. Tribbia, The seasonal cycle over the tropical Pacific in 1293
 coupled ocean–atmosphere general circulation models, *Mon.* 1294
Wea. Rev. 123 (1995) 2825–2838. 1295
- [13] P.S. Schopf, M.J. Suarez, Vacillations in a coupled 1296
 ocean–atmosphere model, *J. Atmos. Sci.* 45 (1988) 549–566. 1297
- [14] D.S. Battisti, A.C. Hirst, Interannual variability in the tropical 1298
 atmosphere/ocean system: influence of the basic state, ocean 1299
 geometry and nonlinearity, *J. Atmos. Sci.* 46 (1989) 1687– 1300
 1712. 1301
- [15] M.J. Münnich, M.A. Cane, S.E. Zebiak, A study of 1302
 self-excited oscillations in a tropical ocean–atmosphere 1303
 system. Part II. Nonlinear cases, *J. Atmos. Sci.* 48 (1991) 1304
 1238–1248. 1305
- [16] M. Cane, S.E. Zebiak, A theory for El Niño and the Southern 1306
 Oscillation, *Science* 228 (1985) 1084–1087. 1307
- [17] D.S. Battisti, The dynamics and thermodynamics of a 1308
 warming event in a coupled tropical atmosphere/ocean model, 1309
J. Atmos. Sci. 45 (1988) 2889–2919. 1310
- [18] F.-F. Jin, J.D. Neelin, Modes of interannual tropical 1311
 ocean–atmosphere interaction: a unified view. I. Numerical 1312
 results, *J. Atmos. Sci.* 50 (1993) 3523–3540. 1313
- [19] A.G. Barnston, H.M. van den Dool, S.E. Zebiak, T.P. Barnett, 1314
 M. Ji, D.R. Rodenhuis, M.A. Cane, A. Leetma, N.E. Graham, 1315
 C.R. Ropelewski, V.E. Kousky, E.A. O'Lenic, R.E. Livezey, 1316
 Long-lead seasonal forecasts — where do we stand? *Bull. Am.* 1317
Meteorol. Soc. 75 (1994) 2097–2114. 1318
- [20] J.D. Neelin, D.S. Battisti, A.C. Hirst, F.-F. Jin, Y. Wakata, T. 1319
 Yamagata, S.E. Zebiak, ENSO theory, *J. Geophys. Res.* 103 1320
 (1998) 14261–14290. 1321
- [21] B. Grieger, M. Latif, Reconstruction of the El Niño attractor 1322
 with neural networks, *Clim. Dyn.* 10 (1994) 267–276. 1323
- [22] F.T. Tangang, W.W. Hsieh, B. Tang, Forecasting the equatorial 1324
 Pacific sea surface temperatures by neural models, *Clim. Dyn.* 1325
 13 (1997) 135–147. 1326
- [23] B. Wang, Y. Wang, Temporal structure of the southern 1327
 oscillation as revealed by wavelets and waveform analysis, *J.* 1328
Clim. 9 (1996) 1586–1598. 1329
- [24] E.M. Rasmusson, X. Wang, C.F. Ropelewski, The biennial 1330
 component of ENSO variability, *J. Mar. Syst.* 1 (1990) 71–96. 1331
- [25] N. Jiang, J.D. Neelin, M. Ghil, Quasi-quadrennial and 1332
 quasi-biennial variability in COADS equatorial Pacific sea 1333
 surface temperature and winds, *Clim. Dyn.* 12 (1995) 101– 1334
 112. 1335

- [26] F. Jacob, J. Monod, Genetic regulatory mechanisms in the synthesis of proteins, *J. Mol. Biol.* 3 (1961) 318–356. 1336
- [27] R. Thomas, *Kinetic Logic: A Boolean Approach to the Analysis of Complex Regulatory Systems*, Springer, Berlin, 1979. 1338
- [28] D. Dee, M. Ghil, Boolean difference equations. I. Formulation and dynamic behavior, *SIAM J. Appl. Math.* 44 (1984) 111–126. 1339
- [29] M. Ghil, A.P. Mullhaupt, Boolean delay equations. II. Periodic and aperiodic solutions, *J. Stat. Phys.* 41 (1985) 125–173. 1340
- [30] F.-F. Jin, J.D. Neelin, M. Ghil, El Niño/Southern Oscillation and the annual cycle: subharmonic frequency locking and aperiodicity, *Physica D* 98 (1996) 442–465. 1341
- [31] M. Ghil, N. Jiang, Recent forecast skill for the El Niño and the Southern Oscillation, *Geophys. Res. Lett.* 25 (1998) 171–174. 1342
- [32] S. Smale, Differentiable dynamical systems, *Bull. Am. Math. Soc.* 73 (1967) 747–817. 1343
- [33] V.I. Arnol'd, *Geometrical Methods in the Theory of Ordinary Differential Equations*, Springer, New York, 1983. 1344
- [34] M. Hénon, La topologie des lignes de courant dans un cas particulier, *CR Acad. Sci. Paris* 262 (1966) 312–414. 1345
- [35] P. Collet, J.-P. Eckmann, *Iterated Maps on the Interval as Dynamical Systems*, Birkhäuser, Basel, 1980. 1346
- [36] S. Wolfram, *Cellular Automata and Complexity: Collected Papers*, Addison-Wesley, Reading, MA, 1994. 1347
- [37] H. Gutowitz, *Cellular Automata: Theory and Experiment*, MIT Press, Cambridge, MA, 1991. 1348
- [38] C. Emiliani, J. Geiss, On glaciations and their causes, *Geol. Rundschau* 46 (1957) 576–601. 1349
- [39] W.S. Broecker, D.M. Peteet, D. Rind, Does the ocean-atmosphere system have more than one stable mode of operation? *Nature* 315 (1985) 21–25. 1350
- [40] J. Imbrie, A. Berger, E.A. Boyle, S.C. Clemens, A. Duffy, W.R. Howard, G. Kukla, J. Kutzbach, D.G. Martinson, A. McIntyre, A.C. Mix, B. Molino, J.J. Morley, L.C. Peterson, N.G. Pisias, W.L. Prell, M.E. Raymo, N.J. Shackleton, J.R. Toggweiler, On the structure and origin of major glaciation cycles 2: the 100,000-year cycle, *Paleoceanography* 8 (1993) 699–735. 1351
- [41] C. Nicolis, Boolean approach to climate dynamics, *QJR Meteorol. Soc.* 108 (1982) 707–715. 1352
- [42] S.A. Kauffman, Metabolic stability and epigenesis in randomly constructed genetic nets, *J. Theoret. Biol.* 22 (1969) 437–467. 1353
- [43] G.A. Cowan, D. Pines, D. Melzer (Eds.), *Complexity: Metaphors, Models and Reality*, Addison-Wesley, Reading, MA, 1994. 1354
- [44] S.A. Kauffman, *At Home in the Universe: The Search for Laws of Self-Organization and Complexity*, Oxford University Press, New York, 1995. 1355
- [45] J. Guckenheimer, P. Holmes, *Nonlinear Oscillations, Dynamical Systems and Bifurcations of Vector Fields*, Springer, Berlin, 1983. 1356
- [46] E.N. Lorenz, Deterministic nonperiodic flow, *J. Atmos. Sci.* 20 (1963) 130–141. 1357
- [47] B. Saltzman, A survey of statistical-dynamical models of the terrestrial climate, *Adv. Geophys.* 20 (1978) 183–304. 1358
- [48] B. Saltzman, Climatic systems analysis, *Adv. Geophys.* 25 (1983) 173–233. 1359
- [49] M. Ghil, S. Childress, *Topics in Geophysical Fluid Dynamics: Atmospheric Dynamics, Dynamo Theory and Climate Dynamics*, Springer, Berlin, 1987 (Chapter 11). 1396
- [50] W.W. Kellogg, Feedback mechanisms in the climate system affecting future levels of carbon dioxide, *J. Geophys. Res.* 88 (1983) 1263–1269. 1397
- [51] M. Ghil, A.P. Mullhaupt, P. Pestiaux, Deep water formation and Quaternary glaciations, *Clim. Dyn.* 2 (1987) 1–10. 1398
- [52] D.G. Wright, T.F. Stocker, L.A. Mysak, A note on Quaternary climate modeling using Boolean delay equations, *Clim. Dyn.* 4 (1990) 263–267. 1399
- [53] M.S. Darby, L.A. Mysak, A Boolean delay equation model of an interdecadal Arctic cycle, *Clim. Dyn.* 8 (1993) 241–246. 1400
- [54] T.S. Saaty, *Modern Nonlinear Equations*, Dover, New York, 1981. 1401
- [55] K. Bhattacharya, M. Ghil, I.L. Vulis, Internal variability of an energy-balance model with delayed albedo effects, *J. Atmos. Sci.* 39 (1982) 1747–1773. 1402
- [56] F.-F. Jin, J.D. Neelin, Modes of interannual tropical ocean-atmosphere interaction: a unified view. II. Analytical results in fully coupled cases, *J. Atmos. Sci.* 50 (1993) 3523–3540. 1403
- [57] J.D. Neelin, The slow sea surface temperature mode and the fast wave limit: analytic theory for tropical inter annual oscillations and experiments in a hybrid coupled model, *J. Atmos. Sci.* 48 (1991) 584–606. 1404
- [58] F.-F. Jin, J.D. Neelin, Modes of interannual tropical ocean-atmosphere interaction: a unified view. III. Analytical results in fully coupled cases, *J. Atmos. Sci.* 50 (1993) 3523–3540. 1405
- [59] F.-F. Jin, Tropical ocean-atmosphere interaction, the Pacific cold tongue, and the El-Niño-Southern Oscillation, *Science* 274 (1996) 76–78. 1406
- [60] P. Chang, B. Wang, T. Li, L. Ji, Interactions between the seasonal cycle and the Southern Oscillation: frequency entrainment and chaos in intermediate coupled ocean-atmosphere model, *Geophys. Res. Lett.* 21 (1994) 2817–2820. 1407
- [61] P. Chang, L. Ji, B. Wang, T. Li, Interactions between the seasonal cycle and El Niño-Southern Oscillation in an intermediate coupled ocean-atmosphere model, *J. Atmos. Sci.* 52 (1995) 2353–2372. 1408
- [62] F.-F. Jin, J.D. Neelin, M. Ghil, El Niño on the Devil's staircase: annual subharmonic steps to chaos, *Science* 264 (1994) 70–72. 1409
- [63] E. Tziperman, L. Stone, M.A. Cane, H. Jarosh, El Niño chaos: overlapping of resonances between the seasonal cycle and the Pacific Ocean-atmosphere oscillator, *Science* 264 (1994) 72–74. 1410
- [64] E. Tziperman, M.A. Cane, S.E. Zebiak, Irregularity and locking to the seasonal cycle in an ENSO prediction model as explained by the quasi-periodicity route to chaos, *J. Atmos. Sci.* 50 (1995) 293–306. 1411
- [65] K. Fraedrich, El Niño/Southern Oscillation predictability, *J. Atmos. Sci.* 116 (1988) 1001–1012. 1412
- [66] T.M. Quinn, T.J. Crowley, F.W. Taylor, C. Henin, P. Joannot, Y. Join, A multicentury stable isotope record from a 1413

- 1452 New Caledonia coral: interannual and decadal sea surface
1453 temperature variability since 1657 AD, *Paleoceanography* 13
1454 (1998) 412–426.
- 1455 [67] E.M. Rasmusson, T.H. Carpenter, Variations in tropical sea
1456 surface temperature and surface wind fields associated with
1457 the Southern Oscillation/El Niño, *Mon. Wea. Rev.* 110 (1982)
1458 354–384.
- 1459 [68] M.H. Jensen, P. Bak, T. Bohr, Transition to chaos by
1460 interaction of resonances in dissipative systems. Part I. Circle
1461 maps, *Phys. Rev. A* 30 (1984) 1960–1969.
- 1462 [69] H.G. Schuster, *Deterministic Chaos: An Introduction*, Physik,
1463 Weinheim, 1988.
- 1464 [70] J.-P. Eckmann, Roads to turbulence in dissipative dynamical
1465 systems, *Rev. Mod. Phys.* 53 (1981) 643–654.
- 1466 [71] P. Bak, R. Bruinsma, One-dimensional Ising model and the
1467 complete Devil’s staircase, *Phys. Rev. Lett.* 49 (1982) 5297–
1468 5308.
- 1469 [72] T. Bohr, P. Bak, M.H.T. Jensen, Transition to chaos by
1470 interaction of resonances in dissipative systems. II. Josephson
1471 junctions, charge-density waves, and standard maps, *Phys.*
1472 *Rev. A* 30 (1984) 1970–1981.
- 1473 [73] M. Ghil, M. Kimoto, J.D. Neelin, Nonlinear dynamics
1474 and predictability in the atmospheric sciences, US National
1475 Report to International Union of Geodesy and Geophysics
1476 1987–1990, *Rev. Geophys. Suppl.* 29 (1991) 46–55.
- 1477 [74] R. Vautard, M. Ghil, Singular spectrum analysis in nonlinear
1478 dynamics with applications to paleoclimatic time series,
1479 *Physica D* 35 (1989) 395–424.
- 1480 [75] M. Ghil, R.M. Allen, M.D. Dettinger, K. Ide, D. Kondrashov,
1481 M.E. Mann, A. Robertson, A. Saunders, Y. Tian, F. Varadi,
1482 P. Yiou, Advanced spectral methods for climatic time series,
1483 *Rev. Geophys.* (2001), in press.
- 1484 [76] C. Penland, P.D. Sardeshmukh, The optimal growth of tropical
1485 sea surface temperatures anomalies, *J. Clim.* 8 (1995) 1999–
1486 2024.
- 1487 [77] C. Penland, A stochastic model of the IndoPacific sea surface
1488 temperature anomalies, *Physica D* 98 (1996) 534–558.
- [78] P. Chang, L. Ji, H. Li, M. Flügel, Chaotic dynamics 1489
versus stochastic processes in the El Niño and the Southern 1490
Oscillation in coupled ocean–atmosphere models, *Physica D* 1491
98 (1996) 301–320. 1492
- [79] E. Tziperman, H. Scher, S.E. Zebiak, M.A. Cane, Controlling 1493
spatiotemporal chaos in a realistic El Niño prediction model, 1494
Phys. Rev. Lett. 79 (1997) 1034–1037. 1495
- [80] N.J. Mantua, S.R. Hare, Y. Zhang, J.M. Wallace, R.C. Francis, 1496
A Pacific interdecadal climate oscillation with impacts on 1497
salmon production, *Bull. Am. Meteorol. Soc.* 78 (1997) 1069– 1498
1079. 1499
- [81] Y.M. Chao, M. Ghil, X. Li, J.C. McWilliams, Pacific 1500
interdecadal variability in this century’s sea surface 1501
temperatures, *Geophys. Res. Lett.* 27 (2000) 2261–2264. 1502
- [82] B.P. Kirtman, P.S. Schopf, Decadal variability in ENSO 1503
predictability and prediction, Report No. 43, Center for 1504
Ocean–Land–Atmosphere Studies, 1997. 1505
- [83] C.J. Zhang, V. Ramanathan, M.J. McPhaden, Convection– 1506
evaporation feedback in the equatorial Pacific, *J. Clim.* 8 1507
(1995) 3040–3051. 1508
- [84] K.-M. Lau, P.H. Chan, Intraseasonal and interannual 1509
variations of tropical convection: a possible link between the 1510
40–50 day oscillation and ENSO, *J. Atmos. Sci.* 45 (1988) 1511
506–521. 1512
- [85] Y. Matsumoto, T. Yamagata, On the origin of a model ENSO 1513
in the western Pacific, *J. Met. Soc. Jpn.* 69 (1991) 197– 1514
207. 1515
- [86] I. Wainer, P.J. Webster, Monsoon–ENSO interaction using 1516
simple coupled ocean–atmosphere model, *J. Geophys. Res.* 1517
101 (1996) 25599–25614. 1518
- [87] D. Gu, S.G.H. Philander, Interdecadal climate fluctuations that 1519
depend on exchanges between the tropics and the extratropics, 1520
Science 275 (1997) 805–807. 1521
- [88] P. Wessel, W.H.F. Smith, Free software helps map and display 1522
data, *Trans. AGU* 72 (1991) 441. 1523
- [89] G. Alefeld, J. Herzberger, *Introduction to Interval Computations*, Academic Press, New York, 1983. 1524
1525